Colloids and Surfaces B: Biointerfaces 262 (2026) 115515

Contents lists available at ScienceDirect

Colloids and Surfaces B: Biointerfaces

journal homepage: www.elsevier.com/locate/colsurfb

# A quality by design study of the use of microfluidic nanoprecipitation for the generation of sub-100 nm drug nanocrystals

Yagmur Pirincci Tok [a,1], Shorooq Abukhamees [a,2], Rawan Fitaihi [a,3], Burcu Demiralp [b], Yildiz Ozsoy [b], Duncan Q.M. Craig [a,*,4]

[a] Research Department of Pharmaceutics, School of Pharmacy, University College London, 29-39 Brunswick Square, London WC1N 1AX, UK
[b] Department of Pharmaceutical Technology, Faculty of Pharmacy, Istanbul University, Istanbul 34116, Türkiye

ARTICLE INFO

*Keywords:*
Antisolvent crystallization
Microfluidic nanoprecipitation
Quality by Design
Solidification
Nanocrystal

ABSTRACT

Although drug nanocrystals have attracted considerable interest within the pharmaceutical industry, there remain issues with the production of nanocrystals with a size below 100 nm. The aim of the present study is to develop a stable, reproducible Canagliflozin (CFZ) sub-100 nm nanosuspension system using microfluidic nanoprecipitation and Quality by Design (QbD) techniques. By means of the circumscribed central composite design (CCCD), critical parameters of the microfluidic nanoprecipitation process and nanosuspension formulation components were optimised. Optimal CFZ nanosuspension with Z-average of 89.52 ± 3.30 nm, PDI of 0.12 ± 0.01 and drug content of 92.49 ± 0.03 % was successfully fabricated using Soluplus as a stabiliser. An increase in saturation solubility corresponding to approximately 250 times the value of the pure CFZ in water was noted. The optimised CFZ nanosuspension was solidified by freeze-drying and electrospraying. Overall, the study has demonstrated that by using a combination of microfluidics and QbD it is promising to generate stable sub-100 nm nanocrystals with high yield, and narrow size distribution and favourable stability.

## 1. Introduction

Nanocrystal technology has become increasingly utilised for enhanced drug bioavailability over recent years due to potentially significant advantages over existing drug delivery strategies such as cyclodextrin inclusion, solid dispersions, micelles, complexation and liposomes [1,2]. These strategies include the requirement for specific physicochemical properties for inclusion into complexes and lipid based nanocarriers [3–5], while liposomal and micellar systems with positive surface charge can cause toxicity due to their immunogenicity. Nanocrystalline systems have attracted interest due to the possibility of augmented saturation solubility, increased dissolution rate and adhesion to cell membranes [6,7]. These systems are essentially carrier free drug particles with a size under 1000 nm, with a structure consisting of pure drug at nanoscale surrounded by a stabilizing layer, thereby theoretically allowing effectively complete drug loading, in turn facilitating high local or circulation concentrations [8]. These advantages can potentially provide a significant opportunity to improve the bioavailability and reduce the side effects of BCS Class II and Class IV drugs [9], in turn allowing reduced dosing compared to conventional forms [10]. On the other hand, as the particle size diminishes below 100 nm, the optimisation of the amount of surfactant required to stabilise the nanosuspension becomes increasingly critical. Insufficient stabilisation can result in aggregation, while excessive stabiliser use may restrict the enhancement of bioavailability [11].

Nanocrystal formulations were estimated to be worth more than $82 billion within the pharmaceutical market in 2021 [12], the majority of products being intended for oral administration [13]. This is a result of their established efficacy when delivered via this route, but also because the difficulty of producing drug nanocrystals with ultrafine particle sizes restricts the use of alternative delivery strategies [14]. For example, the treatment of cancer may require both surface modification of the drug

* Corresponding author.
*E-mail address:* dqmc21@bath.ac.uk (D.Q.M. Craig).
[1] Current address: Department of Pharmaceutical Technology, Faculty of Pharmacy, Istanbul Health and Technology University, Istanbul 34275, Türkiye
[2] Current address: Department of Pharmaceutics and Pharmaceutical Technology, Faculty of Pharmaceutical Sciences,The Hashemite University, Zarqa 13133, Jordan
[3] Current address: Department of Pharmaceutics, College of Pharmacy, King Saud University, Riyadh 11451, Saudi Arabia
[4] Current address: Faculty of Science, University of Bath, Claverton Down, Bath BA2 7AY,UK

https://doi.org/10.1016/j.colsurfb.2026.115515
Received 21 August 2025; Received in revised form 21 December 2025; Accepted 3 February 2026
Available online 4 February 2026

nanocrystals and a particle size range below 100 nm [12]. Moreover, in order to apply the membrane filtration method used to prepare conventionally produced sterile inhalers and parenteral suspensions, the nanosuspension must be of sufficiently small size so as not clog the 0.22 μm pore size filter [15]. There are therefore a range of advantages in being able to successfully produce sub-100nm nanocrystals.

Reducing the size of drug nanocrystals to below 100 nm presents significant technical and thermodynamic challenges, despite offering pharmacological advantages. Within this size range, the dramatic increase in surface energy leads to crystal instability, and processes such as Ostwald ripening cause rapid aggregation and growth of nanocrystals [16]. In terms of production, traditional top-down methods are insufficient for achieving sizes below 100 nm, while traditional bottom-up approaches show limitations in scaling and process control. Top-down methods, especially wet stirred media milling (WSMM), are often preferred by the pharmaceutical industry, whereby the active ingredient particle size can be reduced to 200–400 nm [17,18]. While nanocrystals below 100 nm may be obtained with WSMM, this may necessitate significant extension of the milling process, in turn requiring additional time, energy and hence cost [19]. In addition, contamination of the nanosuspension from ceramic or polymeric bead materials due to bead abrasion must be taken into account [20]. In contrast, most of the drug nanocrystals reported in the literature have been obtained by bottom-up methods, with sizes of less than 100 nm [13]. Amongst the bottom-up technologies, nanoprecipitation is considered to involve low cost and relatively simple scale-up [21,22]. In brief, rapid diffusion of the drug solution into the antisolvent phase generates high supersaturation, in turn leading to precipitation of the drug into submicron particles [23]. A major drawback may be continuation of crystal growth after the precipitation process [24], while rapid and uniform mixing is essential to obtain suitably small particles with a homogenous size distribution [25]. On this basis, typical precipitation methods such as stirred tank mixing and sono-precipitation may be unsuitable for nanocrystal generation due to lack of controlled mixing and precipitation within the process [23,26].

Microfluidics have considerable potential to address the problems associated with conventional antisolvent methods [27]. Although initially utilized as a tool for microanalysis, these methods are now recognized as a sophisticated approach for analysis and fabrication in the pharmaceutical field [28]. The approach may be defined as: "The science and technology of systems that process or manipulate small ($10^{-9}$ to $10^{-18}$ liters) quantities of fluids using channels tens to hundreds of micrometers in size." [29]. Unlike macroscale devices, the laminar flow resulting from the use of micro-channels enables rapid heat and mass transfer [30]. Specific to the study outlined here, the continuous input flow allows consistent and reproducible nanoparticle manufacture, with controlled size, shape, morphology and composition possible, also minimising problems of batch-to-batch variability [31,32].

Fabrication of nanosuspension in microfluidic system involves several operational parameters which may significantly affect outcomes; hence it is crucial to understand and optimise process and formulation variables to obtain stable nanocrystals with appropriate particle characteristics. QbD involves a systematic and statistical approach to systems optimization but also incorporates product and process understanding within predefined objectives based on risk assessment and risk management [33]. This roadmap consists of four main elements, which will be respectively defined as the quality target product profile (QTPP), critical quality attributes (CQAs), critical material attributes (CMAs) and critical process parameters (CPPs) [34].

It is well known that drug nanocrystals in nanosuspension form have a physical stability problem owing to their small particle size. More specifically, the Gibbs free energy dramatically increases when the particle size decreases below 100 nm, leading to high surface energy and hence a tendency to aggregate. In order to achieve optimum stability, drying is often preferred to transform the nanosuspension into a solid phase [35]. Nevertheless, the drying process is of crucial importance with the possibility of crystal growth or aggregation resulting from thermal stress [36]. There exists a number of drying methodologies that may be employed, including centrifugation, freeze-drying, spray-drying, vacuum drying, electrospraying and pellet loading [37,38]. Drying processes become significantly more challenging when the size of the nanocrystals is reduced below 100 nm. The considerably higher surface energy of sub-100 nm particles renders them more susceptible to aggregation, fusion, and irreversible size growth during drying processes [39]. In this study, freeze-drying and electrospraying methods were used to compare the effect of thermal stress on drug nanocrystals; since the first method includes a freezing step while the second method is subjected to electrohydrodynamic process without any heat-related procedure. Here, we investigate the use of both methods to produce a solid form of the nanosuspension under study.

CFZ was used as a model drug in this study. CFZ was launched in 2013 as the first member of sodium glucose co-transporter 2 (SGLT-2) inhibitor approved by FDA [40]. Among antihyperglycemic agents, SGLT-2 inhibitors are notable for their cardiovascular benefits and prevention of renal failure [41,42]. These agents control blood glucose levels independently of insulin by maximizing renal glucose excretion in the proximal tubule of kidney [43]. CFZ is nearly insoluble in aqueous solutions from pH 1.1 and pH 12.9 and is classified as BCS Class IV; the absolute bioavailability is 65 % due to poor to moderate permeability [44]. There are also studies in the literature showing that it could be used in potential treatments for glioblastoma [45], pancreatic [46], lung [47] and thyroid cancer [48], as SGLT-2 is expressed in most cancers.

The main objective of this study is to develop quality controlled and reproducible high yield production of sub-100 nm drug nanocrystals via the use of an inexpensive custom-made Y-shaped microreactor combined with a QbD approach. The synergy between microfluidic nanoprecipitation, facilitating high flow rates, and the QbD approach, providing a methodology for achieving drug nanocrystals with a diameter less than 100 nm, while also having the potential to be further developed into a scalable and industrially relevant protocol. In order to understand the microfluidic nanoprecipitation process (*i.e.* CPP) and to examine the effect of formulation components (*i.e.* CMA), a risk assessment was performed based on pre-formulation studies and literature, and CQAs of the formulation were identified. As part of this main objective, the optimum nanosuspension formulation was converted into solid form using freeze-drying and electrospraying methods for maximum stability, since, as previously mentioned, drug nanocrystals below 100 nm are prone to aggregation.

## 2. Materials and methods

### 2.1. Materials

Canagliflozin (hemihydrate) (CFZ-Hemi) was supplied by Abdi İbrahim Drug Company (Istanbul, Türkiye). Hydroxyl propyl methyl cellulose 6 cP, 15 cP (HPMC, Methocel® E6 LV, Methocel® E15 LV) was obtained from Colorcon Middle East Pvt. Lt. (Istanbul, Türkiye). Soluplus® (Sol), poloxamer 407 (P407, Kolliphor® P407), polyvinylprolidone K30 (PVP K30) were obtained from BASF, Ludwigshafen, Germany.

### 2.2. Preliminary formulation development

Ethanol, in which CFZ is reportedly freely soluble, was used as the organic solvent [49], whereas deionized water, owing to CFZ's low solubility (8.0 μg/mL) [50], was employed as the antisolvent. Pre-formulation studies were carried out using a conventional (in-batch) antisolvent precipitation method by dropwise addition of the solvent phase to the antisolvent phase in a glass vial and continued stirring throughout the process. The effect of varying ratios of the solvent to antisolvent were examined at 1:10, 1:20 and 1:30 *v/v*. Additionally, the effect of different stabilisers such as P407, HPMC E15 and Sol was

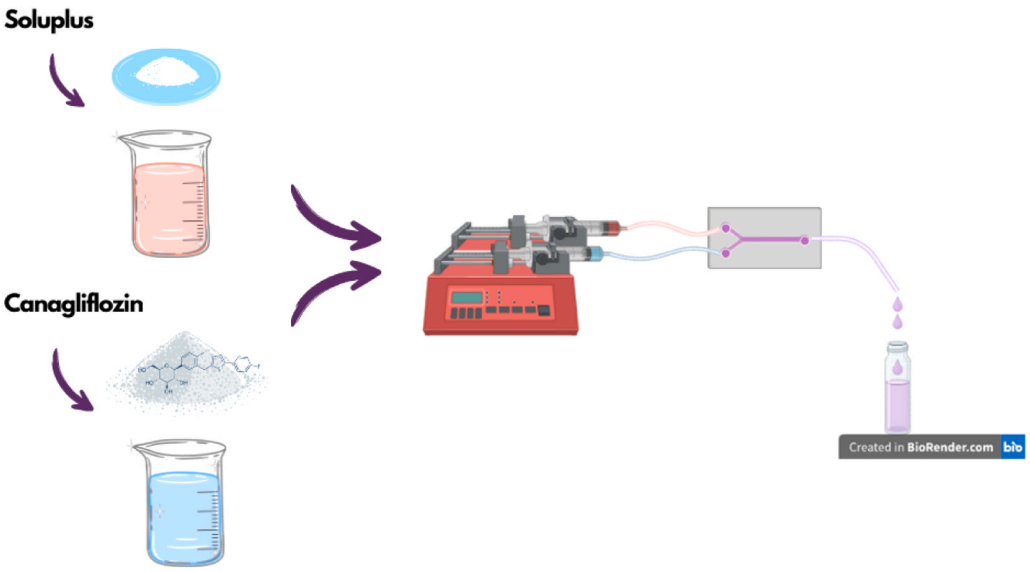


**Fig. 1.** Preparation of CFZ nanosuspension via customized Y-shaped microreactor (Created in https://BioRender.com).

**Table 1**
Examination of formulation and process parameters.

| Formula No. | Drug Conc. in the Solvent Phase (mg/mL) | Soluplus Conc. (*w/v*%) | S:AS ratio | Flow rate (mL/min) |
|---|---|---|---|---|
| **F1** | 200 | 3 | 1:20 | 3.5:70 |
| **F2** | 200 | 3 | 1:15 | 5:75 |
| **F3** | 200 | 4 | 1:20 | 3.5:70 |
| **F4** | 200 | 4 | 1:15 | 4.6:70 |
| **F5** | 200 | 4 | 1:15 | 5:75 |
| **F6** | 300 | 4 | 1:20 | 3.5:70 |
| **F7** | 300 | 4 | 1:15 | 5:75 |

evaluated by dissolving each one separately in water to form antisolvent phase at different concentrations (from 0.125 % to 1.5 %), while the solvent phase was prepared by dissolving varying amounts of CFZ (50, 100 and 150 mg/mL) in ethanol. After obtaining CFZ nanocrystals by the conventional precipitation method (with Sol identified as the most suitable stabiliser as outlined in Section 3) continuous nanocrystal fabrication was explored using microfluidic technology.

The nanocrystals were produced using a custom-made Y-shaped micro-reactor, which was 3D printed (Stereolithography (SLA) printer, Formlab USA) from transparent resin. The inner diameter of the reactor is 0.646 μm ± 0.025 μm, the reaction chamber length is 30 mm, the inlet chamber length is 7 mm, the angle between the inlets is 90 °, and the overall length is 5.4 cm. Pre-cooled (4 °C) Sol solution as the antisolvent solution and solvent solution were prepared as mentioned above and then filtered through a 0.22 μm PES Syringe Filter (Sartorius AG, Germany). They were loaded into gas-tight syringes (SGE) and were pump into the micro reactor inlets at different flow rates using a syringe pump (33 Dual Drive System, Harvard Apparatus, USA), so that the two fluids faced each other in the reaction chamber and precipitated through high supersaturation (Fig. 1). Nanosuspensions with different concentrations of both Sol and CFZ were prepared at various flow rate (60, 70 and 75 mL/min).

As part of the QbD approach, the drug concentration, polymer concentration, solvent:antisolvent (S:AS) ratio and flow rates were examined to determine potential factors and to perform initial risk assessment. The concentration of Sol was investigated from 0.5 % to 3 % by keeping drug concentration in the solvent phase (100 mg/mL) and S:AS ratio (3:60) constant at initial step of the formulation development. In order to increase the amount of drug in the nanosuspension, the concentration of the drug in ethanol was tested from 200 mg to 500 mg/mL. Increasing the drug concentration in the solvent phase from 200 mg/mL to 250 mg/mL, then to 400 mg/mL and 500 mg/mL resulted in an increase in particle size (Z-average) of 90.35 ± 3.51, 116.30 ± 4.35, 134.00 ± 0.87 and 146.30 ± 1.61, respectively. The day after nanosuspension preparation, the particle size of samples with drug concentrations of 400 and 500 mg/mL could not be measured due to Ostwald ripening and aggregation. Further studies were performed with drug concentrations of 200 and 300 mg/mL in the solvent phase to gain insight into the effects of factors on responses (Table 1).

### 2.3. QbD approach for optimization of microfluidic nanoprecipitation

#### 2.3.1. Identifying QTPP and CQAs

The QTPP establishes the starting point of design for the desired drug product. It should meet quality attributes relevant to patient needs, *i.e.,* safety and efficacy of the drug. A potential CQA can be a biological, microbiological, chemical or physical specification which has a critical impact on the product quality and it should be defined within a specific limit, range or distribution [51].

The QTPP elements and CQAs were evaluated in the light of information based on literature review and especially preliminary studies, as shown in Table 2. QTPP has been identified to produce CFZ nanosuspension with particle size below 100 nm, since the decrease in particle size usually results in a significant increase in saturation solubility and dissolution rate, and thus oral bioavailability is expected to improve [52].

In this study, a holding period of 1 week is sufficient to monitor the stability of the nanosuspensions to be solidified to evaluate the behaviours of nanocrystals. Since nanosuspensions are thermodynamically unstable systems they tend to aggregate through Ostwald ripening over time, resulting in changes particle size, solubility properties and ultimately reducing bioavailability. For maximum stability, both chemically and physically, they are usually transformed into solid form [53]. However, the drying process also involves thermal stress, which causes the aggregation of nanocrystals [54]. Therefore, the holding time prior to drying process is essential to gain insight into the nanocrystal behaviour, which might be destabilised during the solidification process. As part of the physical stability evaluation, the mean particle size and PDI of the nanosuspensions prepared according to the experimental design were measured at room temperature and refrigerator conditions after one week.

**Table 2**
QTPP and CQAs of CFZ nanosuspension.

| QTPP Elements | Target | Criticality | Justification |
|---|---|---|---|
| **Dosage form** | Nanosuspension | - | Canagliflozin is a BCS Class IV molecule. The formulation of a nanosuspension has been identified as a promising approach to increase bioavailability, as has been confirmed in the literature for numerous poorly water-soluble drugs [17,55]. |
| **Route of administration** | Oral | - | This is a non-invasive method with high patient compliance, and from the perspective of the pharmaceutical industry, the production of solid dosage forms administered via this route is easier [56]. |
| **Strength** | 100 mg | - | The dose of CFZ is limited to 100 mg once daily in patients with moderate renal impairment with an eGFR of 45 to less than 60 mL/min/1.73 $m^2$ [57]. |
| **Physical stability** | One week | Yes | A duration of one week is sufficient to evaluate the storage stability of the nanosuspensions prior to the drying process, as the nanosuspension is an intermediate product [58]. |
| **Quality attributes of the drug product** | | | |
| **Physical attributes (appearance, odor)** | Milky liquid, no unpleasant odor | No | Physical characteristics were not assessed critically as they were not directly related to safety and efficacy [59]. |
| **pH** | 6.5–7* *any preservative added | No | Oral suspensions are sensitive to pH changes due to exposure to atmospheric carbon dioxide. However, in our study, it was determined that the nanosuspension components CFZ and Sol neutralised the formulation's pH and that the pH remained unchanged throughout the pre-formulation study. Therefore, this was not considered critical. |
| **Zeta Potential** | $\geq \pm 20$ mV for steric<br>$\geq \pm 30$ mV for electrostatic stabilization | No | Zeta potential is often considered as a metric to assess the physical stability of colloidal dispersions. However, this functionality was not observed in the present study. The non-ionic nature of Sol and the neutral nature of CFZ in aqueous solutions did not significantly affect the zeta potential [60]. Preliminary studies showed that the nanosuspensions were stable for at least two weeks, although the zeta potential had negative values close to zero. Therefore, zeta potential was not considered critical. |
| **Particle size (z-average)** | $<$ 100 nm | Yes | As the particle size decreases, oral bioavailability increases due to improvement saturation solubility and dissolution rate according to Kelvin – Ostwald Freundlich and Noyes – Whitney equations [50], thus particle size highly affects therapeutic efficacy. |
| **PDI** | $<$ 0.3 | Yes | The PDI value is indicative of the alteration in the particle size distribution of a nanocrystal suspension, and is influenced by its physical stability. A PDI value higher than 0.5 indicates a broad particle size distribution and the possibility of Ostwald ripening; this causes a decrease in the drug's solubility and dissolution rate, and consequently a reduction in its bioavailability [16]. It has been critically assessed as having a significant impact on effectiveness. |
| **Assay** | % 90 - %110 | Yes | The assay constitutes a specific and stability-indicating test, the purpose of which is to determine the potency (content) of the drug product [61]. It has been critically assessed as it directly affects effectiveness and safety. |

### 2.3.2. *Risk assessment after preliminary formulation development*

The CMAs and CPPs are linked to CQAs via a risk assessment process that helps define formulation and process parameters [62]; the potential effects of the parameters on the product quality can be analysed by identifying and ranking them using risk assessment tools. Failure Mode Effects Analysis (FMEA) was preferred to estimate risks related to specified hazards, as shown in Table 3. As a quantitative method, the approach numerically indicates the probability (P) of occurrence and severity (S) of harm and its detectability (D), thus a Risk Priority Number (RPN) can be calculated, as shown in the following equation [63].

RPN= Probability (P) x Severity (S) x Detectability (D)

Each unit can be ranked from 1 to 9 where the number of 1 stand for minimal, unlikely and certain in terms of severity, probability and detectability, respectively and while the number 9 means significant, highly likely and unlikely.

**Table 3**
Risk assessment for CFZ nanosuspension based on FMEA tool.

| Failure Mode | Failure Cause | Failure Effects | P | S | D | RPN | Strategy |
|---|---|---|---|---|---|---|---|
| **Concentration of CFZ** | Inability to understand formulation development | Nanosuspension may not occur, nanosuspension at the desired particle size is not obtained, Insufficient drug content for therapeutic effectiveness, cannot provide sufficient increase in saturation solubility thus resulting in inadequate bioavailability and drug performance | 6 | 9 | 4 | 216 | Determining the appropriate amount of drug |
| **Concentration of Sol** | Inability to understand formulation development | Unacceptable particle size, polydisperse system, physical instability, inadequate bioavailability. | 7 | 9 | 4 | 252 | Determining the appropriate amount of Sol |
| **Ratio of solvent to antisolvent** | Inability to monitor the process | Unacceptable particle size, polydisperse system, physical instability, inadequate bioavailability | 1 | 8 | 1 | 8 | Determined by preliminary studies. |
| **Flow rate** | Inability to monitor the process | Unacceptable particle size, polydisperse system, physical instability, inadequate bioavailability | 5 | 8 | 4 | 160 | Determining the appropriate most appropriate flow rate |

**Table 4**
Variables in the experimental design.

| **Independent Variables** | **Levels** | | | | |
|---|---|---|---|---|---|
| | -α | -1 | 0 | +1 | +α |
| $X_1$: Concentration of CFZ in solvent phase (mg/mL) | 165.9 | 200 | 250 | 300 | 334.1 |
| $X_2$: Concentration of Sol in antisolvent phase (% w/v) | 2.659 | 3 | 3.5 | 4 | 4.341 |
| $X_3$: Flow rate (mL/min.) | 59.56 | 60 | 65 | 70 | 73.41 |
| **Responses** | **Desirable Goals** | | | | |
| $Y_1$: Particle size (Z- average, nm) | < 100 | | | | |
| $Y_2$: PDI | Minimize | | | | |
| $Y_3$: Drug content | Maximize | | | | |
| $Y_4$: Particle size (7 day at 4 °C) | Minimize | | | | |

**Table 5**
CCC design scheme for CFZ nanosuspension.

| Exp. Name | Run Order | $X_1$ (mg/mL) | $X_2$ (w/v%) | $X_3$ (mL/min.) |
|---|---|---|---|---|
| **N1** | 16 | 200 | 3 | 60 |
| **N2** | 11 | 300 | 3 | 60 |
| **N3** | 8 | 200 | 4 | 60 |
| **N4** | 4 | 300 | 4 | 60 |
| **N5** | 2 | 200 | 3 | 70 |
| **N6** | 17 | 300 | 3 | 70 |
| **N7** | 7 | 200 | 4 | 70 |
| **N8** | 12 | 300 | 4 | 70 |
| **N9** | 1 | 165.9 | 3.5 | 65 |
| **N10** | 15 | 334.1 | 3.5 | 65 |
| **N11** | 5 | 250 | 2.659 | 65 |
| **N12** | 6 | 250 | 4.341 | 65 |
| **N13** | 14 | 250 | 3.5 | 56.59 |
| **N14** | 13 | 250 | 3.5 | 73.41 |
| **N15** | 10 | 250 | 3.5 | 65 |
| **N16** | 3 | 250 | 3.5 | 65 |
| **N17** | 9 | 250 | 3.5 | 65 |

### 2.3.3. Experimental design for optimization of sub-100 nm CFZ nanosuspension

Circumscribed central composite design (CCCD) within response surface methodology (RSM) was utilized to optimize nanosuspension formulation and microfluidic process, and to assess the interaction of the factors on each response (*i.e.,* CQAs). The experimental design was established by Minitab® 19 statistical software. The largest process space within 5 levels (-α, −1, 0, +1, +α) of each of the three factor was examined by means of CCCD with 8 factorial points, 6-star points and 3 centre points. Alpha value was adjusted to 1.682. Extreme points for each factor's low and high values were made to create star points. The independent factors with their levels and the responses corresponding to their combinations are presented in Table 4.

In order to enhance the model's predictability, all experimental runs were conducted randomly. The resulting data were then evaluated via ANOVA regression within the Minitab® 19 software. The second-order polynomial model equation which is shown as mentioned below (1) was employed to examine the effects of the factors on the dependent responses (CQAs).

$$(Y) = \beta_0 + \beta_1X_1 + \beta_2X_2 + \beta_3X_3 + \beta_{12}X_1X_2 + \beta_{13}X_1X_3 + \beta_{23}X_2X_3 + \beta_{11}X_{21} + \beta_{22}X_{22} + \beta_{33} \times X_{23}. \quad (1)$$

Where, Y refers to response associated with the combination at each factor level; $\beta_0$ is an intercept; $X_1$, $X_2$ and $X_3$ are the coded levels of independent variables. βi's' and 'βii's' (i = 1–3) are the coefficients of individual linear and quadratic effects of the variables [64].

### 2.4. Characterization of CFZ nanosuspension

#### 2.4.1. Measurements of particle size and poly-dispersibility index (PDI)

Particle size (Z-average) and PDI value were measured by dynamic light scattering technique using a Zetasizer Nano ZS instrument (Malvern Instruments, UK) at a detection angle of 173 ° at 25 °C [65]. All measurements were performed in triplicate without any dilution.

#### 2.4.2. Drug content analysis

The CFZ content in both the experimental design samples and the optimal nanosuspension was analysed by UV-Spect. (Agilent Cary 100 UV-Vis Spectrophotometer) at 290 nm. The assay method was validated regarding specificity, linearity and range, detection limit and quantification limit, accuracy and recovery. The amount of CFZ in nanosuspension was analysed by dissolving CFZ nanosuspension equivalent to 5 mg CFZ (50 μg/mL) in methanol [66]. The samples were sonicated for 3 min. and filtered with 0.20 μm RC filters (Sartorius AG, Germany).

#### 2.4.3. Short-term physical stability

Short-term physical stability for both DoE samples and optimal nanosuspension was performed to examine the nanosuspension stability. Particle size (Z-average) and PDI were measured after storing for 7 days at room temperature (25 ± 2 °C) and in the refrigerator (4 ± 2 °C), as the optimal nanosuspension would be converted into solid form.

#### 2.4.4. Saturation solubility

The saturation solubility studies were conducted for coarse powder of CFZ and optimal nanosuspension by the shake-flask method. To assess their surface-active properties, an excess amount of CFZ was added to the dispersion medium in a vial with and without surfactants. The vials were shaken at 100 rpm for 48 h at room temperature. After 48 h, the samples were centrifuged at 15000 rpm for 30 min and the supernatants were filtered by 0.20 μm RC filters for separating filtrate. They were analysed using a UV assay method after appropriate dilution.

### 2.5. Solidification of optimal CFZ nanosuspension

The optimum nanosuspension was converted to the solid form for maximum stability. In this study two drying techniques were evaluated to transform the nanosuspensions into powders, namely freeze-drying and electrospraying. The organic solvent in the optimal nanosuspension was removed by evaporation method using rotary

evaporator (Buchi, United Kingdom) under 102 mbar at 50 °C [67]. The effect of the solvent evaporation process on nanosuspension quality was monitored by measuring the particle size and PDI value before and immediately after the process, and one day later. Additional trials were conducted at 80 °, 70 ° and 60 °C (Table S1) to find the best evaporation temperature, it was decided to keep the temperature at 50 °C.

#### 2.5.1. Freeze-drying method

Mannitol was used as a cryoprotectant, as it is widely used for drying nanosuspensions; as a water-soluble compound, it forms a matrix around the nanocrystals and dissolves after rehydration, allowing the primary nanoparticles to re-form [68]. Mannitol was added to the mixture at a concentration of 1.33 % *w/v*. The final mixture was frozen in a laboratory freezer (-20 °C) for at least 12 h and then immediately freeze-dried for 48 h (Thermo Fisher Scientific, MicroModulyo 1.5 L freeze dryer).

#### 2.5.2. Electrospraying technique

The optimal CFZ nanosuspension was dried via electrospraying using a Spraybase® system (Dublin, Ireland) as an alternative method for freeze-drying. Electrospraying has been applied for drying nanoparticles in recent years [69]. As it is an electrohydrodynamic atomization technique, the final mixture is charged due to high-voltage while passing through the nozzle, thus being sprayed from the nozzle tip to the collective device under static electric field [70]. While mannitol was added to final mixture to improve bulkiness and compressibility features of electrosprayed powder [34], PVP K30 was used in the electro-spraying procedure due to its particle-forming capacity [71]. The process parameters were set as follows: the distance between the nozzle tip and the collector was 20 cm, the flow rate was 0.2 mL/h and the applied voltage was 20 kV.

#### 2.5.3. Characterization of dried nanocrystals

*2.5.3.1. SEM analysis.* The raw CFZ and dried nanosuspension samples were analysed for morphology using scanning electron microscopy (SEM) FEI Quanta 200 FEG (FEI, USA). The samples were attached onto aluminum SEM stubs (TAAB Laboratories, UK) using a carbon-coated double-sided tape and a thin coating of gold was applied in a Quorum Q150T sputter coater (Quorum Technologies Ltd. East Sussex, UK) in an argon atmosphere to make them conductive.

*2.5.3.2. Characterization of solid-state nanocrystals.* Thermal properties of Canagliflozin, Sol, physical mixture (PM), and optimized dried nanosuspension with/without mannitol were characterized with DSC analysis using TA Instruments DSC Q2000 equipped with a finned-air cooler (New Castle, USA). Accurately weighed 5 mg of sample was placed in hermetically sealed aluminium pans, and exposed to heating at 10 °C/min in the range of 25–200 °C under nitrogen purge gas flow (50 mL/min). An empty crimped pan was used as a reference. The crystalline properties of the optimized dried nanosuspension were examined using a bench-top diffractometer (Rigaku Miniflex 600, Japan). XRD patterns of CFZ, Sol, PMs, optimized dried nanosuspension with/without mannitol and were taken at a scan rate of 5 °C/min in the range of 0–45 °

## 3. Results and discussion

### 3.1. Preliminary formulation development

Nanosuspensions could only be produced using Sol as the stabilizer. This may be due to the low viscosity of its solutions at the concentrations used compared to HPMC-E15, allowing greater supersaturation through effective mixing, resulting in a higher nucleation rate and smaller particle size [72]. Similarly, although Sol and P407 are both amphiphilic polymers, formulations with P407 resulted in visible particle aggregation, possibly due to Sol exhibiting superior steric hindrance than P407 [73]. This can be explained by the much stronger hydrophobic interactions between the cyclic structures in CFZ and the lactam rings in Sol.

**Table 6**
Evaluation of preliminary nanosuspension in terms of particle size and PDI.

| Formula No. | Particle size (nm ± SD) | PDI (nm ± SD) |
|---|---|---|
| F1 | 139.10 ± 1.50 | 0.19 ± 0.02 |
| F2 | 165.90 ± 1.57 | 0.19 ± 0.05 |
| F3 | 98.32 ± 0.94 | 0.10 ± 0.01 |
| F4 | 115.70 ± 4.10 | 0.18 ± 0.01 |
| F5 | 146.40 ± 3.85 | 0.17 ± 0.02 |
| F6 | 112.70 ± 2.95 | 0.15 ± 0.01 |
| F7 | 153.70 ± 0.50 | 0.15 ± 0.01 |

The nanosuspension with the smallest particle size of 98.32 nm was produced with 4 % Soluplus® at a S:AS ratio of 1:20 and 70 mL/min when the drug concentration in the solvent phase was 200 mg/mL, as shown in Table 6. However, when the S:AS ratio was increased from 1:20–1:15, particle size increased to 115.70 nm. As anticipated, an increase in the S:AS ratio resulted in a reduction in the supersaturation level, which in turn led to a decline in the nucleation rate and an increase in the particle size [74].

It was also observed that the flow rate had a significant ($p < 0.0001$) effect on the particle size. More specifically, at 1:15 S:AS ratio, when the flow rate was increased from 4.6:60 mL/min to 5:75 mL/min, the particle size increased from 115.70 nm to 146.4 nm. In theory, a higher flow rate is required to facilitate an efficient, homogeneous mixing process in which greater supersaturation is achieved between the diffusion layers of these two fluid streams [75]. The process of effective mixing has been demonstrated to result in a reduction in the time required for the crystallisation of active pharmaceutical ingredients, with the formation of drug nanocrystals occurring at a faster rate [76]. In our case, the observed increase in particle size with increasing flow rate may be attributed to an increase in the solvent flow rate. This led us to hypothesize that the polymer concentration was insufficient to achieve complete coverage of the CFZ nanocrystalline particles. Moreover, consistent with the study by Gajera et al. [77] increasing drug concentration with increasing polymer concentration resulted in an increase in particle size.

It was observed that increasing the amount of polymer with increasing drug concentration was not sufficient to obtain stable nanocrystals. Considering all the preliminary experimental results, it was decided to apply the quality by design approach to obtain the optimal CFZ nanosuspension with the smallest particle size, higher stability and drug content.

### 3.2. QbD approach for optimization of microfluidic nanoprecipitation

Based on the initial risk analysis using the FMEA approach, the potentially critical parameters were identified as flow rate, polymer and drug concentrations. The question of whether these parameters may have a significant impact on CQAs was analysed using a design within the framework of RSM.

#### 3.2.1. Circumscribed central composite design for optimization of sub-100 nm CFZ nanosuspensions

CCC design is widely used under the umbrella of RSM, consisting of mathematical and statistical methodology to reveal the influence of independent factors on dependent factors (responses) within the boundaries of experimental design, thereby facilitating understanding of the interaction between them, thus optimising the formulation components and the manufacturing process on an empirical model [78,79]. To achieve these objectives, 17 experimental designs were prepared according to the CCC matrix and CFZ nanosuspensions were prepared at

**Table 7**
Response variables and observed values from CCC design.

| Exp. Name | Particle size ($Y_1$) (Z-ave, nm) | PDI ($Y_2$) | Drug Content ($Y_3$, %) | Part. size after 1 week at 4 °C ($Y_4$, Z-ave, nm) |
|---|---|---|---|---|
| N1 | 126.80 | 0.18 | 91.35 | 93.39 |
| N2 | 128.10 | 0.11 | 78.51 | 115.10 |
| N3 | 100.40 | 0.15 | 93.93 | 88.71 |
| N4 | 125.40 | 0.18 | 83.76 | 102.20 |
| N5 | 124.60 | 0.16 | 93.02 | 93.22 |
| N6 | 129.70 | 0.12 | 79.48 | 127.60 |
| N7 | 101.60 | 0.11 | 92.40 | 85.90 |
| N8 | 133.30 | 0.16 | 82.81 | 105.10 |
| N9 | 111.90 | 0.13 | 82.73 | 82.88 |
| N10 | 138.40 | 0.10 | 44.96 | 97.72 |
| N11 | 128.50 | 0.12 | 84.73 | 114.90 |
| N12 | 132.60 | 0.20 | 81.62 | 91.79 |
| N13 | 129.20 | 0.19 | 80.99 | 98.08 |
| N14 | 131.40 | 0.18 | 82.88 | 101.90 |
| N15 | 141.30 | 0.19 | 83.53 | 102.90 |
| N16 | 149.60 | 0.18 | 82.17 | 99.87 |
| N17 | 151.20 | 0.19 | 83.31 | 107.00 |

**Table 8**
Summary of regression analysis of each response.

| Response Variables | S | R-sq | R-sq (adjusted) |
|---|---|---|---|
| $Y_1$ | 7.172 | 88.34 % | 73.36 % |
| $Y_2$ | 0.013 | 92.98 % | 47.58 % |
| $Y_3$ | 0.004 | 73.00 % | 38.30 % |
| $Y_4$ | 5.739 | 88.94 % | 74.72 % |

different CFZ, Sol and flow rate levels and the nanosuspensions were characterised in terms of particle size, PDI, drug content and stability (particle size at day 7 and 4 °C) as presented in Table 7. As part of evaluation of physical stability, particle size at room temperature and PDI values at both room temperature and refrigerator conditions are shown in Table S1, supplementary material.

A multiple regression analysis was carried out in order to examine the relationship between the independent variables and the responses in an empirical model. The summary of the regression analysis for each response is presented in Table 8.

The S-value is one of the indicators of model quality and represents the average difference between the experimental responses and the fitted values. The regression coefficient (R-sq) is always between 0 and 1 (*i.e.*, between 0 % and 100 %) and reflects the proportion of variability explained by the model. The relatively lower adjusted $R^2$ value observed for $Y_3$ (drug content) compared to the corresponding $R^2$ is mainly related to the intrinsic characteristics of this response. Although the model explains a considerable proportion of the overall variability ($R^2 \approx 73$ %), regression analysis indicated that drug content is less sensitive to formulation and process-related factors than the other responses as illustrated Fig. 2 (c). Under such conditions, the inclusion of multiple model terms relative to the number of experimental runs leads to a reduction in the adjusted $R^2$, as this metric penalizes statistically insignificant contributions. Therefore, the lower adjusted $R^2$ reflects the limited dependence of drug content on the selected independent variables rather than deficiencies in experimental execution, analytical methodology, or model adequacy.

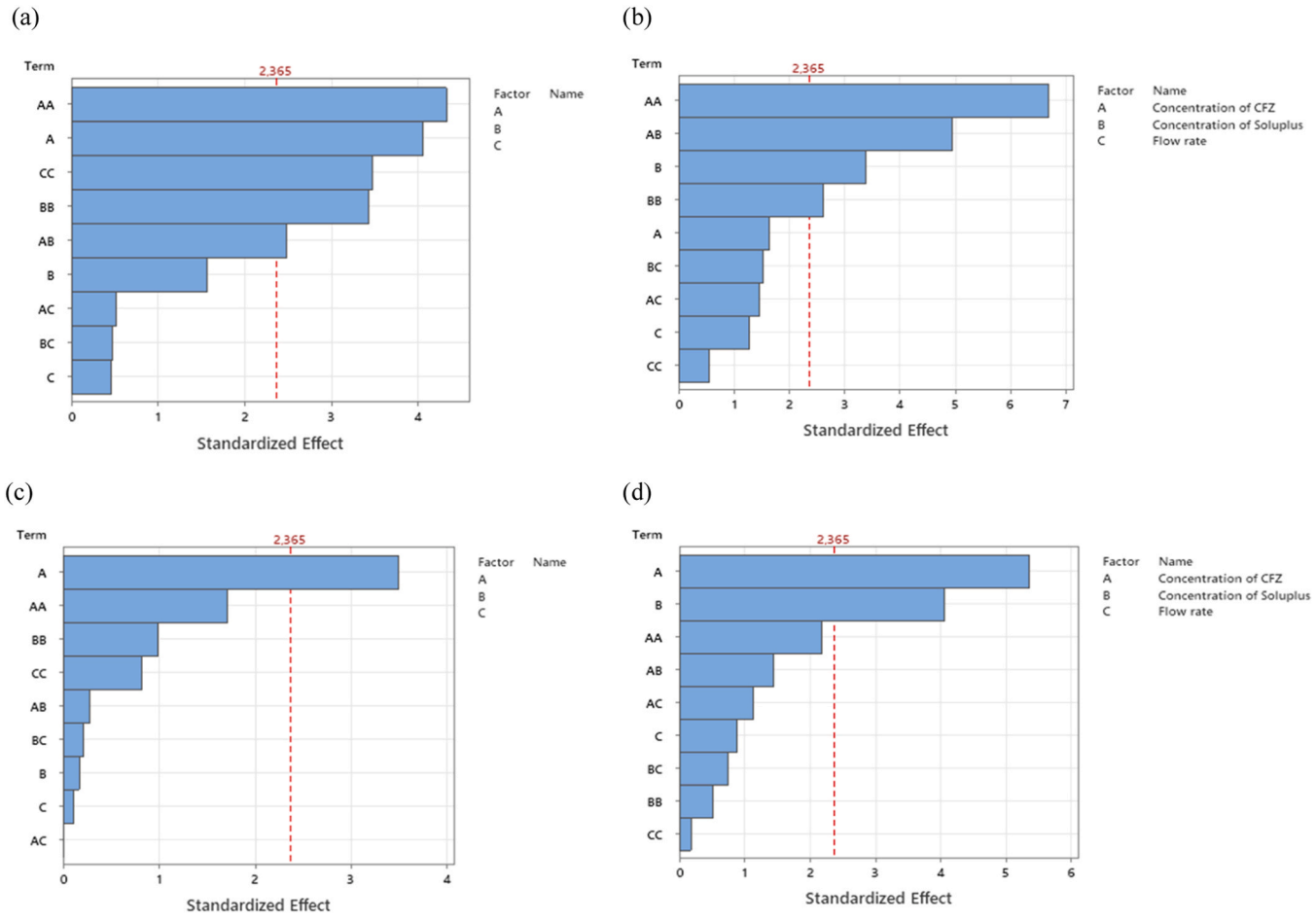


**Fig. 2.** Pareto charts of standardized effect for each Response; (a): particle size, (b): PDI, (c): drug content, (d): particle size after 1 week at 4 °C. α= 0.05. Terms: A= Concentration of CFZ in solvent phase, B= Concentration of Soluplus in antisolvent phase, C= Flow rate.

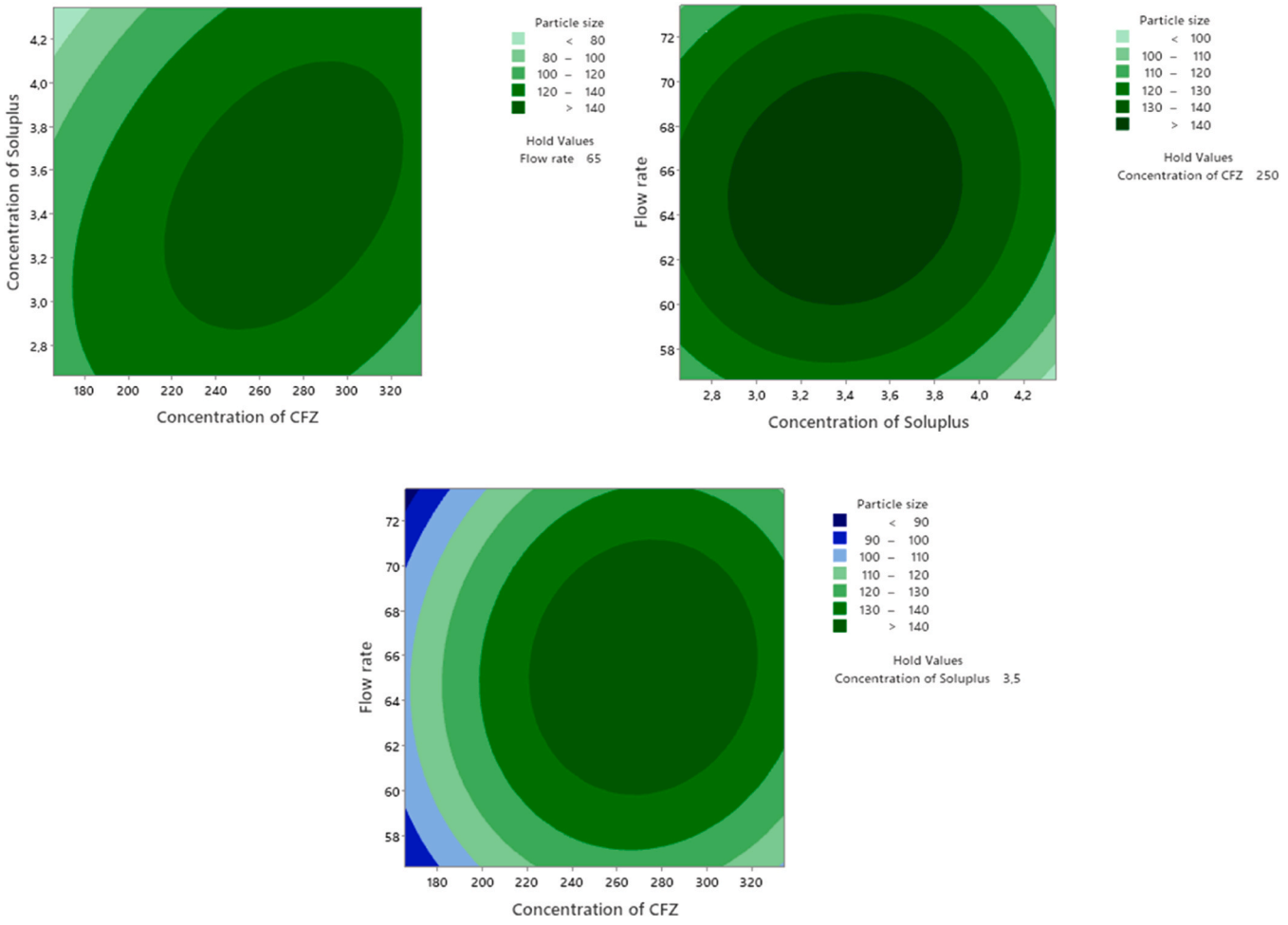


**Fig. 3.** 2- way interactions of each factor together effect of factors on particle size.

### 3.2.2. *Effect of independent factors on responses*

The effect of independent factors on particle size (Z-average): The Pareto charts are presented in Fig. 2, with the bars ordered from highest to lowest frequency. This allows the independent factors to be displayed in order of importance for each response, from the most significant to the least. As can be seen in Fig. 2(a), the squared terms of drug concentration (referring to AA), flow rate (referring to CC) and Sol concentration (referring to BB) have a statistically significant effect on the particle size of the nanosuspension with $p$ values of 0.003, 0.010 and 0.011, respectively. A linear interaction of drug concentration and a 2-way interaction of drug concentration/Sol concentration (referring to AB) have a significant effect on particle size with $p$ values of 0.005 and 0.042, respectively.

The particle size of the nanosuspensions in the design experiments ranged from 101.60 to 151.20 nm (Table 7). Interestingly, the nanosuspensions with the largest particle size were found at the centre of the independent factors as seen Fig. 3 (a, b, c). Similarly, a study by Henriquez et al. [80] showed that nanosuspensions with the largest particle

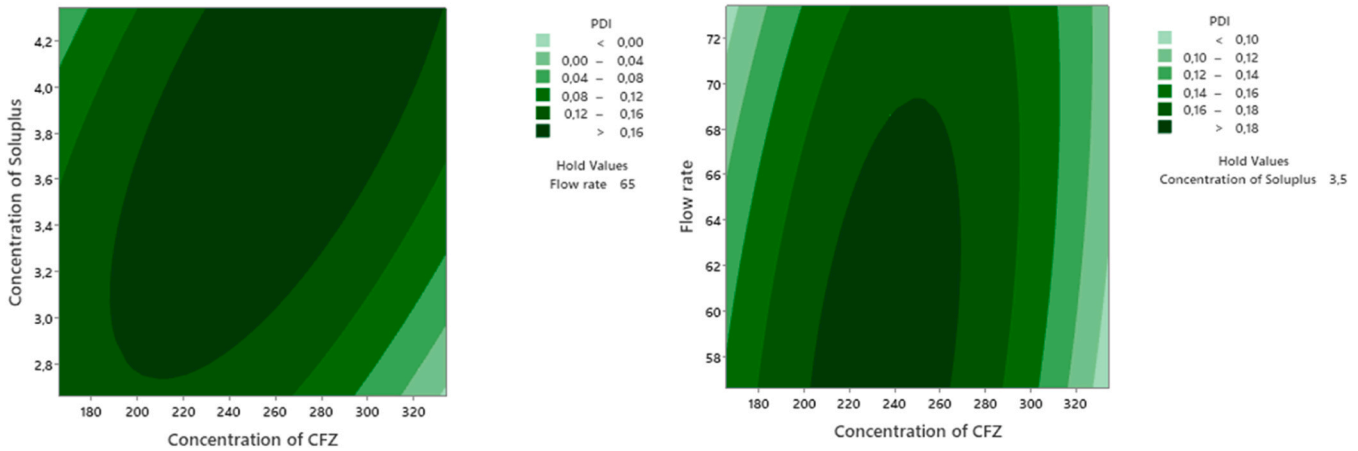


**Fig. 4.** 2- way interactions of each factor together on PDI value.

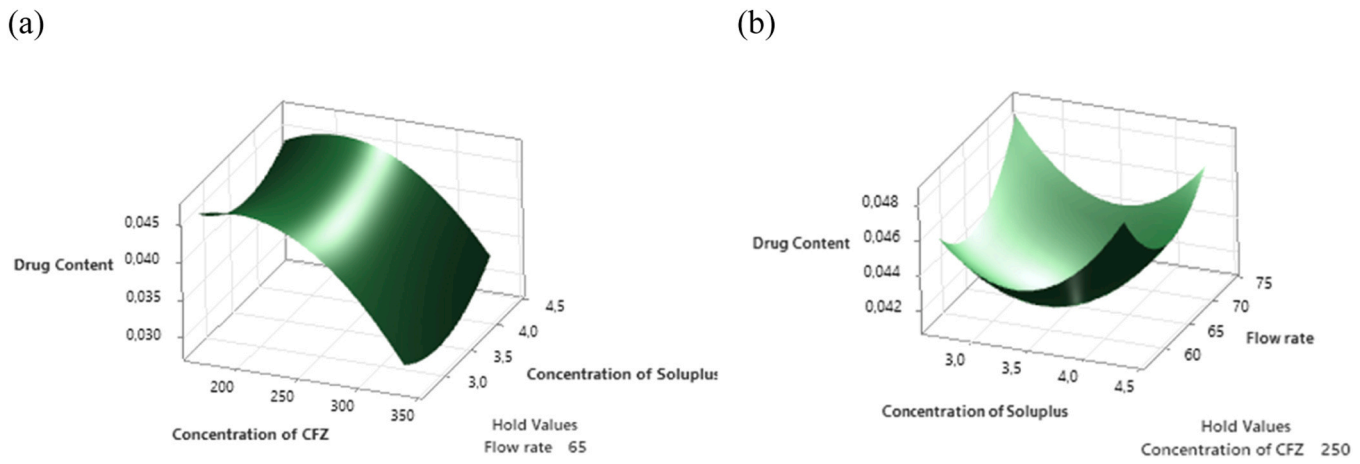


**Fig. 5.** Effect of independent factors on drug content.

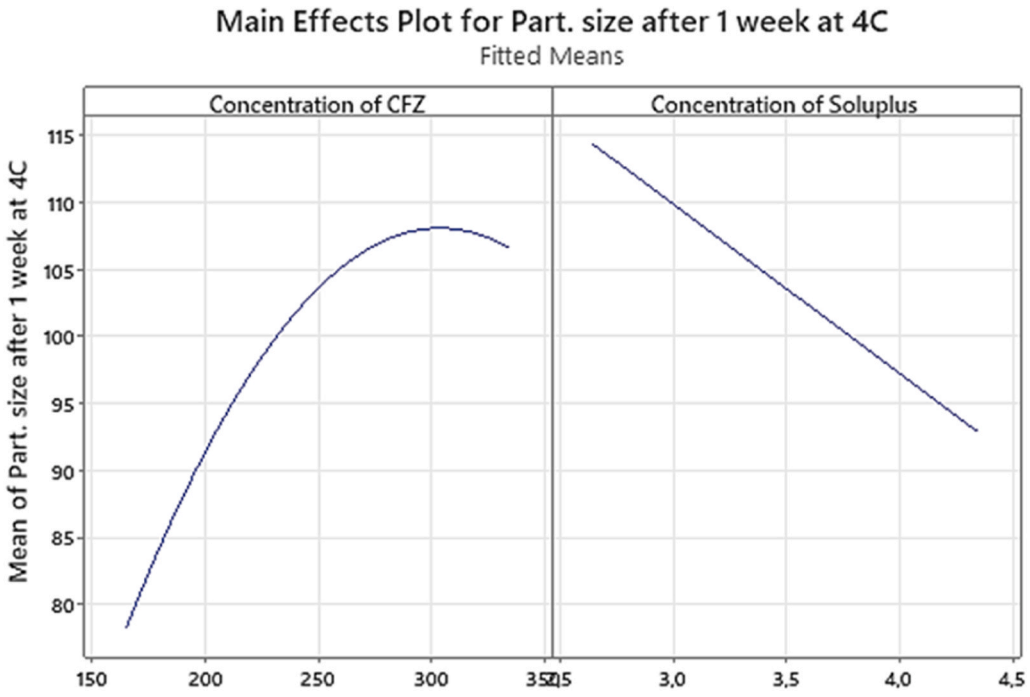


**Fig. 6.** Main effect plot for particle size after 1 week at 4 °C.

size were at the centre of the factors. As shown in Fig. 2 (a), the nanosuspension with the smallest particle size below 80 nm can be obtained at the lowest drug concentration and the highest Sol concentration. In other words, the increase in Sol concentration has resulted in greater surface coverage of the nanocrystals. Furthermore, Fig. 2(c) shows that no matter how high or low the flow rate is, it has no significant effect on the particle size at low drug concentration, as the particle size is below 90 nm at both levels of flow rate. This can also be understood from 2-way interaction of CFZ concentration in solvent phase and flow rate (referring to AC) in pareto chart of particle size (Fig. 2(a), since the interaction was below the red line.

The effect of independent factors on PDI: The quadratic terms of drug and Sol concentration, the 2-way interaction of these two terms and the linear interaction of Sol concentration have a significant effect on PDI with p values of 0.000, 0.002, 0.012 and 0.035 respectively (Fig. 2 (b)). Similar to the situation with particle size, the highest PDI values were observed at the centres of the drug and Sol concentrations (Fig. 4).

Effect of independent factors on drug content: The drug content of the nanosuspension was significantly influenced by the only independent factor, the drug concentration (Fig. 2(c)). RSM examination of the curvature (Fig. 5 (a)) shows that the drug content initially increases with increasing drug concentration in the solvent phase from 165 mg/mL to around 200 mg/mL, but further increase in drug concentration resulted in a decrease in drug content, probably due to particle growth, agglomeration and deterioration of the nanosuspension structure [81]. This deterioration may be indicative of the outcome of experiment 10, where nanosuspension with the highest drug concentration exhibited the lowest level of unusual drug content. A higher drug ratio may have favoured crystal growth by condensation.

Effect of independent factors on the particle size after 1 week at 4 °C: Significant linear effects of CFZ and Sol concentrations on particle size over time were clearly seen, with *p*-values of 0.001 and 0.005, respectively (Fig. 2 (d)). At higher drug concentrations, an increase in particle size was observed in the first instance, followed by a slight decrease in particle size. A decreasing trend in particle size was observed with increasing Sol concentration (Fig. 6). This can be explained by the fact

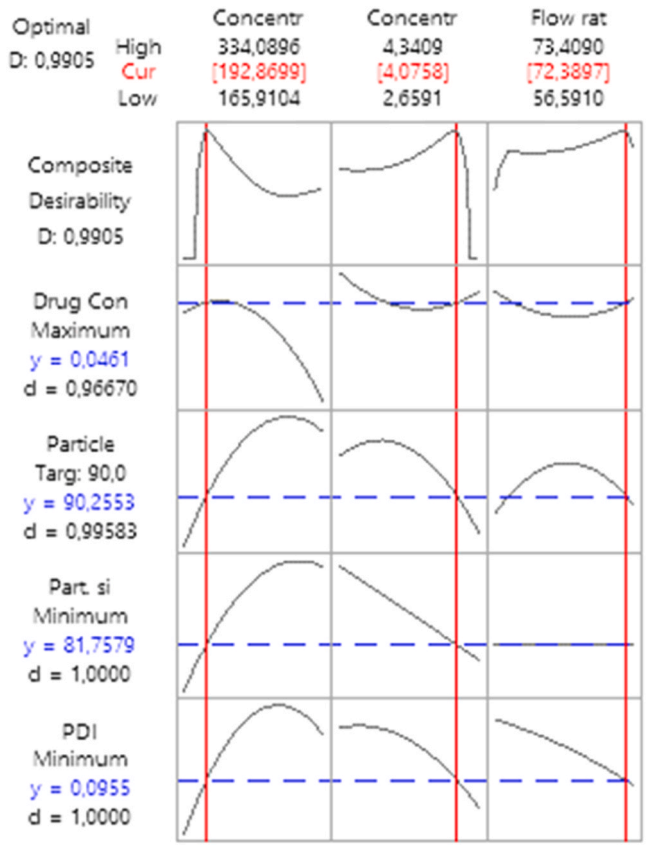


**Fig. 7.** Optimization plot of CFZ nanosuspension produced by microfluidic nanoprecipitation.

**Table 9**
Predicted and observed values of CQAs of CFZ nanosuspension.

| | Responses | | | |
|---|---|---|---|---|
| | Particle size (nm) | PDI | Drug Content (%) | Part. size after 1 week at 4 °C (Stability) |
| Predicted | 90.26 | 0.10 | 92.30 | 81.76 |
| Observed | 89.52 ± 3.30 | 0.12 ± 0.01 | 92.49 ± 0.03 | 87.33 ± 2.02 |

that a higher concentration of polymer can cover the drug nanocrystals more easily than a lower concentration of polymer [77].

The effect of room temperature on the physical stability of CFZ nanosuspensions prepared by the DoE method was also investigated. The particle size and PDI values were much higher than those stored at 4 °C (Fig. S1). This could be evidence that the ambient temperature stimulates particle growth and Ostwald ripening due to increased drug solubility and increased diffusion to the particle boundary layer. Furthermore, as the temperature increases, the viscosity of the water decreases, leading to triggered particle growth due to increased molecular transport rates and particle collisions [82]. In light of the aforementioned observation and the effect of temperature, it can be posited that the conversion of drug nanocrystals in colloidal dispersion into a solid form offers optimal stability throughout the shelf life.

### 3.3. Optimization and validation for desired Canagliflozin nanosuspension

The relationship of independent factors with the responses has been demonstrated on empirical models, and in this section, an optimization study has conducted to obtain nanosuspension with desired CQAs. The aim was to develop a CFZ nanosuspension with a particle size of less than 100 nm, minimum PDI, highest drug content and stability at least for 1 week. The settings of the independent factors are determined by the optimisation strategy, which uses empirical models to help achieve the predefined CQAs. The optimisation plot (Fig. 7) shows the optimal levels of the independent factors and the predicted responses of the CQAs with high desirability (0.99). The proposed levels of formulation components and process parameters were used to compare predicted and observed responses and ultimately validate the DOE approach for the production of optimised nanosuspensions.

As can be seen in Table 9, the agreement between the results of predicted and observed responses indicates that DOE is a reliable approach to achieve the predefined CQAs of CFZ nanosuspensions prepared by microfluidic nanoprecipitation.

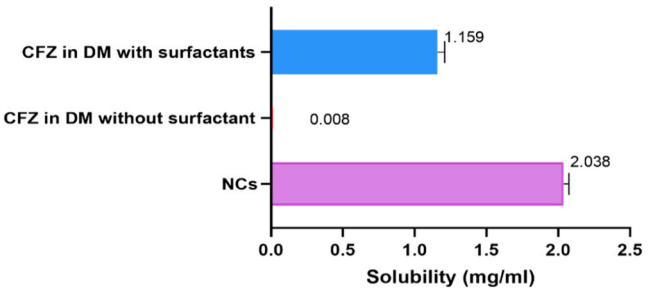


**Fig. 8.** Saturation solubility of pure CFZ in different media and optimal nanosuspension.

### 3.4. Characterization of optimal nanosuspension and its solidified forms

The measurements of solubility studies and drug content of the nanosuspension were conducted with a validated assay method of CFZ. The linearity range was between 5 and 60 μg/mL, and the limit of detection (LOD) and limit of quantification (LOQ) were calculated as 1.086 μg/mL and 3.296 μg/mL, respectively. The calibration curve (Figure S1), together with the regression equation and coefficient, for the assay method of CFZ, and the accuracy and percent recovery (Table S2) were presented in the supplementary material.

The particle size, PDI value, drug content (%), and stability (measured as the particle size after one week of storage at 4 °C), were determined using the previously described methods. The corresponding results are presented in Table 9.

#### 3.4.1. Saturation solubility

Nanocrystal technology is an effective way of improving saturation solubility owing to the increase in particle curvature and the resultant dissolution pressure, as given by the Kelvin equation [83]. The solubility of CFZ in the dispersion medium without surfactant was 0.008 mg/mL, while the solubility in the medium containing surfactant was 1.159 mg/mL (Fig. 8). Sol increased the solubility of API due to the associated surface-active properties. The solubility of CFZ in nanosuspension in nanocrystalline form was found to be 1.758 times better than that of pure CFZ in the dispersion medium containing Sol at the same concentration as optimized nanosuspension. The findings indicated that the use of nanocrystal technology facilitated the improved solubility of drug particles in comparison to the use of surfactants.

*3.4.2. SEM analysis.* SEM was used to assess the morphology of CFZ nanocrystals following electrospraying and freeze-drying processes. Fig. 9 presents SEM images of electrosprayed samples at various magnifications (200 μm to 2 μm), while Fig. 10 shows corresponding images of freeze-dried samples (20 μm to 1 μm). For comparison, SEM images of pure CFZ are provided in the supplementary material (Fig. S2).

The electrosprayed nanocrystals appeared more uniformly dispersed and exhibited a predominantly spherical morphology. This may be

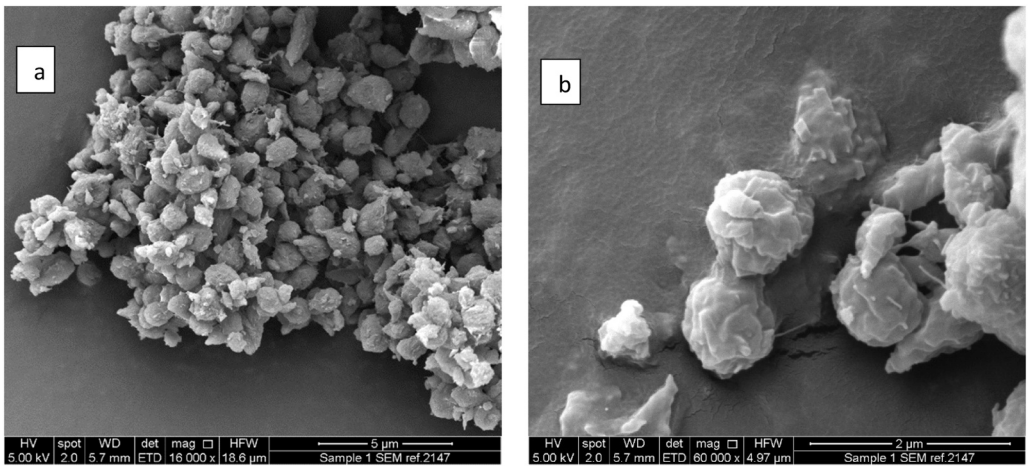


**Fig. 9.** SEM images of electrosprayed nanocrystals scaled at, a) 5 µm, b) 2 µm.

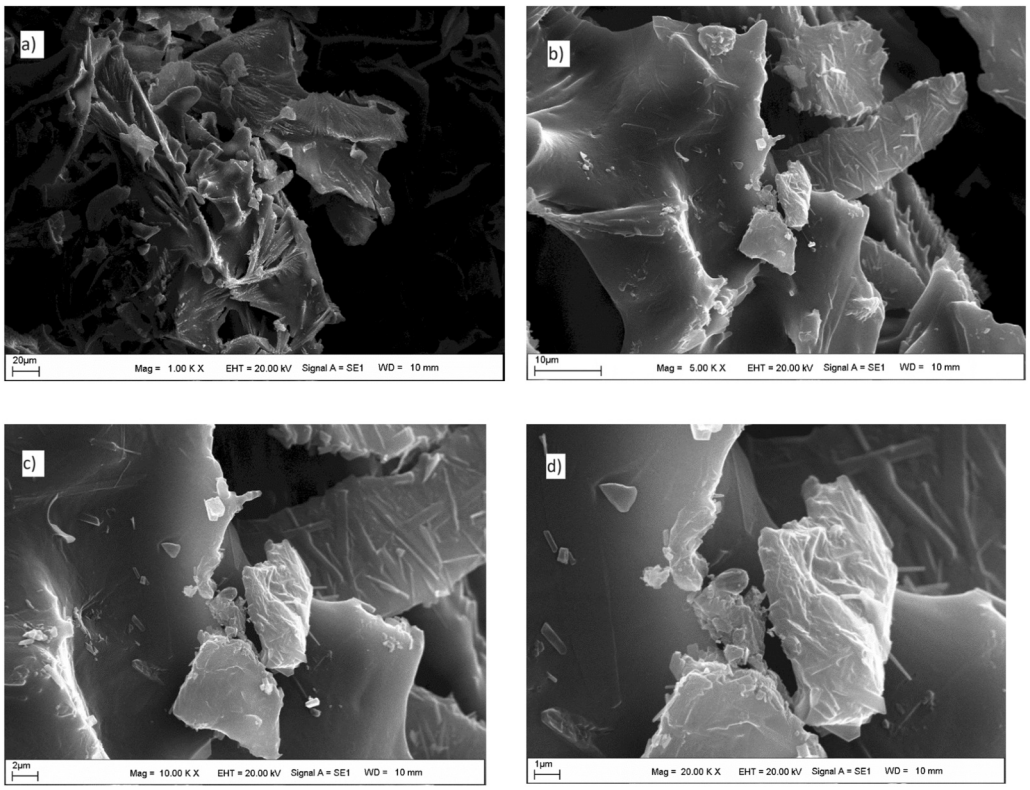


**Fig. 10.** SEM images of frieze dried nanocrystals scaled at a) 20 µm, b) 10 µm, c) 2 µm, d) 1 µm.

attributed to the slower solvent evaporation characteristic of electrospraying, allowing adequate time for nanocrystal diffusion from the surface toward the particle core. According to the Peclet number model, when the solvent evaporation rate is lower than the solute diffusion rate (Pe $<$ 1), more uniform and spherical particles are likely to form [84, 85].

In contrast, the freeze-dried samples showed signs of structural collapse and agglomeration, with irregularly shaped particles. This deterioration is likely a result of thermal stress encountered during the freezing and secondary drying steps of the freeze-drying process, which can reduce interparticle distance and disrupt steric stabilization. These observations indicate that both the drying method and the choice of excipients (e.g., PVP K30 and mannitol) significantly influence the morphology of the final nanocrystals [36]. The electrosprayed formulations, which incorporated both excipients, exhibited superior particle uniformity compared to the freeze-dried samples prepared with mannitol alone.

Fig. 10 clearly demonstrates the deterioration in the structure of the particles, ultimately the agglomeration of the system and irregular shape and view. Freeze drying process involves thermal stress, as a consequence of freezing and secondary drying steps [37]. Under the influence of these thermal stresses, termination of the interparticle distance and loss of steric stabilisation can be observed.

The SEM analysis clearly demonstrates that the morphology of the nanocrystals is dependent on the drying method and excipients (i.e. PVP K30 and mannitol) employed in each process. The electrosprayed nanocrystals produced using PVP K30 and mannitol exhibited greater uniformity in size and morphology compared to the freeze-dried

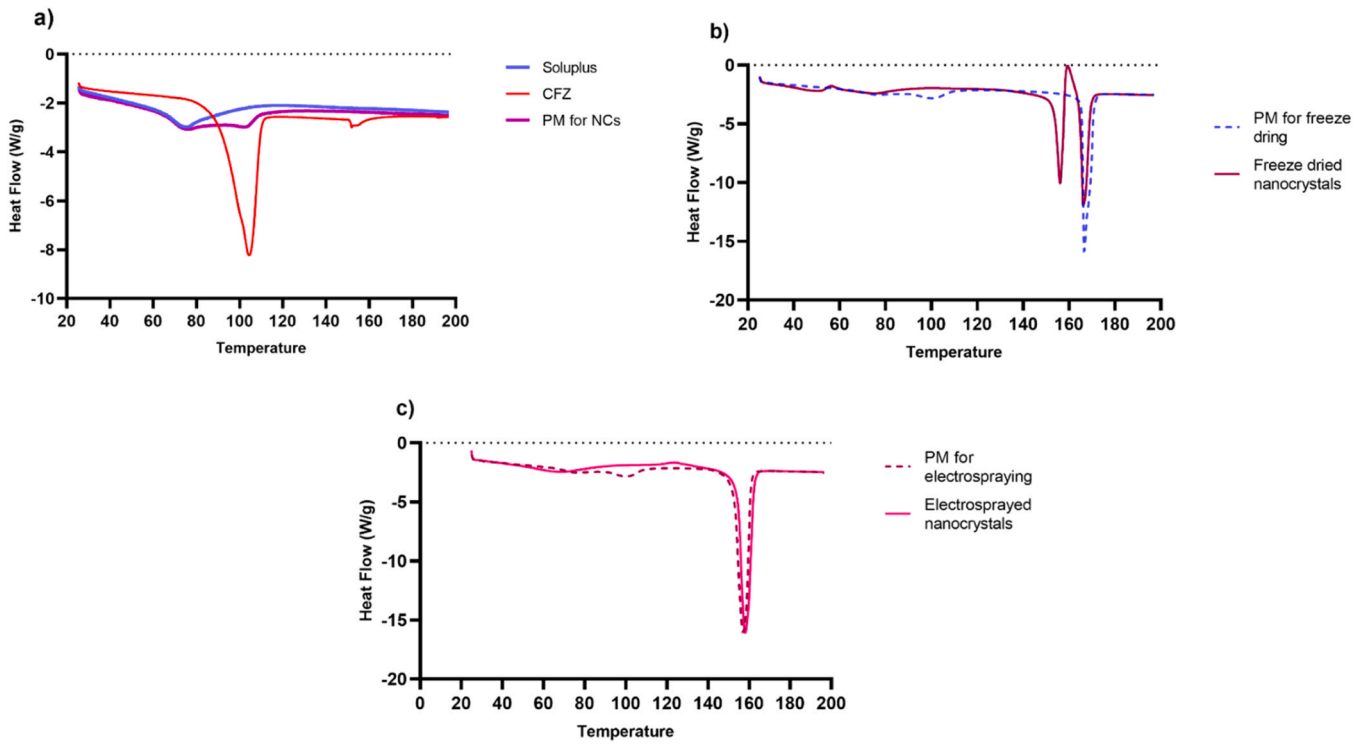


**Fig. 11.** DSC thermograms of CFZ, Soluplus, PMs and dried nanocrystals.

nanocrystals containing mannitol. Furthermore, the freeze-drying process was conducted using PVP K30 in combination with mannitol as a cryoprotectant. Nonetheless, upon the rehydration and subsequent measurement of this freeze-dried nanosuspension through DLS, a higher particle size (4100 ± 640 nm) and PDI value (0.45 ± 0.04) was obtained (for graphs see Fig. S3 in supplementary material). This may be

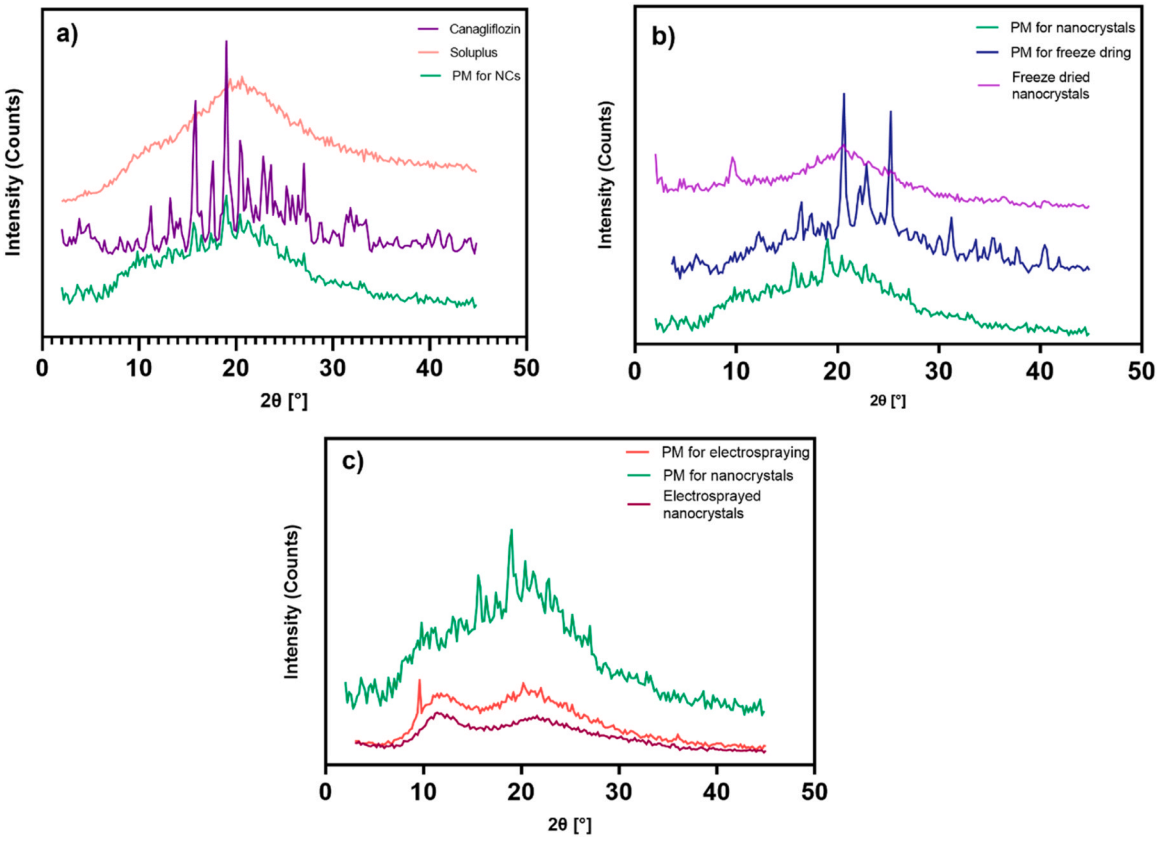


**Fig. 12.** XRD diffractograms of CFZ, Soluplus, PMs and dried nanocrystals.

attributed to a freeze-concentrated phase forms as the solution concentrates. While mannitol, used as a cryoprotectant, undergoes crystallization, PVP-K30 does not form a crystalline structure; instead, it concentrates in the non-freezing (liquid) phase. This can lead to a heterogeneous microstructure and phase separation. In these heterogeneous structures, nanocrystals can exhibit size increase after aggregation and redispersion by being compressed in changing environments or assembling in the polymer-rich amorphous phase [86].

Finally, the hydrated particle sizes measured after resuspending the samples in deionised water provide confirmation of the SEM images. The nanosuspension subjected to electrospray drying returned to its original particle size, while the nanosuspension subjected to freeze-drying reached micrometre dimensions (Fig. S4 and Fig. S5 in supplementary material).

### 3.4.3. Analysis of solid-state characteristics

DSC was employed to evaluate the thermal behavior and crystallinity of various CFZ samples, including pure CFZ hemihydrate, Sol, physical mixtures (PMs), and dried nanocrystals produced via freeze-drying and electrospraying (Fig. 11). The DSC thermogram of CFZ hemihydrate exhibited a sharp endothermic peak at 104.40 °C, consistent with its known melting point, indicating a crystalline structure. Sol displayed a thermal event at 75.64 °C, corresponding to its glass transition temperature (Tg), which aligns with its amorphous nature [87]. The physical mixtures showed two characteristic peaks: one corresponding to CFZ and another for mannitol at 166.51 °C (Figs. 11b and 11c). Notably, in both dried nanocrystal formulations, the CFZ melting peak was absent, suggesting a transition from crystalline to amorphous form during processing. This transformation is consistent with previous studies reporting that nanoprecipitation, particularly under high supersaturation, can lead to amorphization of poorly water-soluble drugs [23,88,89].

Furthermore, mannitol polymorphism was evident in the freeze-dried nanocrystals (Fig. 11b). An endothermic peak at 156.08 °C was followed by an exothermic event and a second endothermic peak at 166.14 °C, which may indicate the presence of metastable δ-mannitol transforming into its more stable α- or β-forms upon heating [90]. In contrast, electrosprayed samples (Fig. 11c) exhibited only a single mannitol peak, suggesting limited or no polymorphic transformation under the electrospraying conditions.

PXRD was conducted to examine the crystallinity of CFZ formulations and support findings from DSC (Fig. 12). The pure CFZ sample exhibited intense, well-defined diffraction peaks at 2θ values of 11.13 °, 13.25 °, 15.75 °, 17.55 °, 19.01 °, 20.53 °, 21.27 °, 22.81 °, 23.63 °, 25.35 °, and 26.99 °, confirming its crystalline structure. These results are consistent with previously reported PXRD patterns for CFZ [91]. As expected, Sol displayed a broad halo pattern, indicative of its amorphous character [92]. The physical mixtures maintained the primary CFZ diffraction peaks but with diminished intensity, reflecting a reduction in CFZ content due to dilution with excipients (Figs. 12a–c). In contrast, both freeze-dried and electrosprayed nanocrystal formulations (Figs. 12b and 12c) exhibited the absence of characteristic CFZ peaks, with PXRD patterns transitioning to diffuse halos. This loss of crystallinity further supports the inference from DSC that CFZ underwent a crystalline-to-amorphous transition during nanoprecipitation and subsequent drying.

## 4. Conclusion

This study demonstrated that drug nanocrystals below 100 nm can be easily produced by means of the combined application of microfluidic nanoprecipitation and QbD methods. The optimal nanosuspension showed a mean particle size and PDI of 89.52 ± 3.30 nm and 0.12 ± 0.01, respectively instead of 90.26 nm and 0.10 for the predicted value by QbD. The predicted drug content (%) and particle size after 1 week at 4 °C (in terms of stability) were 92.3 %, 87.33 ± 2.02 nm, respectively, while the observed values were 92.49 % and 81.76 nm. These results suggest that the predicted and observed results of the CQAs (responses) were mainly correlated, demonstrating that the QbD roadmap is a reliable and reproducible approach. It is also noteworthy that as a result of the optimisation study, the nanosuspension production flow rate increased to 75 mL/min. This finding can be considered promising in terms of scalability, but of course the residual solvent problem inherent in the antisolvent precipitation technique should be taken into account. As a result of the optimisation study, a CFZ nanosuspension with stable, repeatable, cost-effective and narrow particle size distribution was prepared which showed a 1.76-fold higher solubility than pure CFZ in dispersion media with Sol, whereas it showed 254.74-fold higher solubility than in distilled water. The optimised CFZ nanosuspension was converted into a solid form by freeze-drying and electrospraying for maximum stability. The SEM images in this study have also contributed to the literature on electrospraying as a solidification technique for nanosystems, as the particles dried by this method were spherical and more uniform than those dried by freeze-drying. However, the industrial applicability of electrospraying needs to be improved, due to the low flow rate (0.2 mL/min.) resulting from the aqueous nature of the nanosuspension. This improved saturation solubility is expected to increase the dissolution rate, bioavailability and reduce the daily dose, as these parameters are related, as stated in the Noyes-Whitney equation, the Kelvin equation and as shown in numerous literatures. Further studies are required to investigate the reconstitution and stability of dried CFZ nanocrystals under different physiological conditions, ultimately to convert them into a final dosage form and then to investigate the relationship between particle size and bioavailability.

## CRediT authorship contribution statement

**Duncan Q.M. Craig:** Writing – review & editing, Project administration, Conceptualization. **Yildiz Ozsoy:** Writing – review & editing, Methodology, Investigation, Formal analysis, Conceptualization. **Burcu Demiralp:** Writing – review & editing, Methodology, Investigation, Formal analysis, Conceptualization. **Rawan Fitaihi:** Writing – review & editing, Methodology, Investigation, Conceptualization. **Shorooq Abukhamees:** Writing – review & editing, Visualization, Methodology, Investigation. **Yagmur Pirincci Tok:** Writing – review & editing, Writing – original draft, Methodology, Conceptualization.

## Declaration of Competing Interest

The authors declare the following financial interests/personal relationships which may be considered as potential competing interests: Yagmur Pirincci Tok reports a relationship with The Scientific and Technological Research Council of Türkiye (TUBITAK) that includes: funding grants. If there are other authors, they declare that they have no known competing financial interests or personal relationships that could have appeared to influence the work reported in this paper.

## Acknowledgments

Yagmur Pirincci Tok would like to thank the International Research Fellowship Programme for PhD Students (The Scientific and Technological Research Council of Türkiye - 2214/A) for the scholarship provided program (grant number: 1059B142200207).

## Appendix A. Supporting information

Supplementary data associated with this article can be found in the online version at doi:10.1016/j.colsurfb.2026.115515.

## Data availability

Data will be made available on request.

## References


[1] J. Che, Y. Fu, Y. Li, Y. Zhang, T. Yin, J. Gou, X. Tang, Y. Wang, H. He, Eudragit L100-coated nintedanib nanocrystals improve oral bioavailability by reducing drug particle size and maintaining drug supersaturation, Int. J. Pharm. 658 (2024) 124196, https://doi.org/10.1016/j.ijpharm.2024.124196.

[2] M. Imono, H. Uchiyama, S. Yoshida, S. Miyazaki, N. Tamura, H. Tsutsumimoto, K. Kadota, Y. Tozuka, The elucidation of key factors for oral absorption enhancement of nanocrystal formulations: in vitro–in vivo correlation of nanocrystals, Eur. J. Pharm. Biopharm. 146 (2020) 84–92, https://doi.org/10.1016/j.ejpb.2019.12.002.

[3] A. Junnila, L. Mortier, A. Arbiol, E. Harju, T. Tomberg, J. Hirvonen, T. Viitala, A. P. Karttunen, L. Peltonen, Rheological insights into 3D printing of drug products: drug nanocrystal-poloxamer gels for semisolid extrusion, Int. J. Pharm. 655 (2024) 124070, https://doi.org/10.1016/j.ijpharm.2024.124070.

[4] N. Jabeen, M. Sohail, A. Mahmood, S.A. Shah, A.H.M. Qalawlus, T. Khaliq, Nanocrystals loaded collagen/alginate-based injectable hydrogels: a promising biomaterial for bioavailability improvement of hydrophobic drugs, J. Drug Deliv. Sci. Technol. 91 (2024) 105291, https://doi.org/10.1016/j.jddst.2023.105291.

[5] Y. Wang, H. Li, L. Wang, J. Han, Y. Yang, T. Fu, H. Qiao, Z. Wang, J. Li, Mucoadhesive nanocrystal-in-microspheres with high drug loading capacity for bioavailability enhancement of silybin, Colloids Surf. B Biointerfaces 198 (2021) 111461, https://doi.org/10.1016/j.colsurfb.2020.111461.

[6] J. Liu, S. Qu, T. Wang, B. Yang, X. Liu, G. Wang, P. Li, Q. Yu, F. Ling, Nanosuspensions as an approach for improved solubility and anti-Ichthyophthirius multifiliis activity of magnolol, Aquaculture 579 (2024) 740133, https://doi.org/10.1016/j.aquaculture.2023.740133.

[7] P.S. Chary, S. Shaikh, V. Bhavana, N. Rajana, R. Vasave, N.K. Mehra, Emerging role of nanocrystals in pharmaceutical applications: a review of regulatory aspects and drug development process, Appl. Mater. Today 40 (2024) 102334, https://doi.org/10.1016/j.apmt.2024.102334.

[8] E. Zingale, A. Bonaccorso, C. Carbone, T. Musumeci, R. Pignatello, Drug nanocrystals: focus on brain delivery from therapeutic to diagnostic applications, Pharmaceutics 14 (2022) 691, https://doi.org/10.3390/pharmaceutics14040691.

[9] H. Awad, M. Rawas-Qalaji, R.E. Hosary, J. Jagal, I.S. Ahmed, Formulation and optimization of ivermectin nanocrystals for enhanced topical delivery, Int. J. Pharm. X 6 (2023) 100210, https://doi.org/10.1016/j.ijpx.2023.100210.

[10] A. Rossetti, D.A. Real, B.A. Barrientos, D.A. Allemandi, A.J. Paredes, J.P. Real, S. D. Palma, Significant progress in improving Atorvastatin dissolution rate: physicochemical characterization and stability assessment of self-dispersible Atorvastatin/Tween 80® nanocrystals formulated through wet milling and freeze-drying, Int. J. Pharm. 650 (2024) 123720, https://doi.org/10.1016/j.ijpharm.2023.123720.

[11] M. Alkhaldi, C.M. Keck, Challenges, unmet needs, and future directions for nanocrystals in dermal drug delivery, Molecules 30 (15) (2025) 3308, https://doi.org/10.3390/molecules30153308.

[12] V. Jarvis, S. Krishnan, Mitragotri, Nanocrystals: a perspective on translational research and clinical studies, Bioeng. Transl. Med. M (2018) 5–16, https://doi.org/10.1002/btm2.10122, 24.

[13] L.D.O. Macedo, J.F. Masiero, N.A. Bou-Chacra, Drug nanocrystals in oral absorption: factors that influence pharmacokinetics, Pharmaceutics 16 (2024) 1141, https://doi.org/10.3390/pharmaceutics16091141.

[14] B. Rossier, O. Jordan, E. Allémann, C. Rodriguez-Nogales, Nanocrystals and nanosuspensions: an exploration from classic formulations to advanced drug delivery systems, Drug Deliv. Transl. Res. 14 (2024) 3438–3451, https://doi.org/10.21203/rs.3.rs-3621399/v1.

[15] C.J. Carling, A. Pekkari, Bead milled drug nanocrystal suspensions fine enough to pass through 0.22 μm sterilization filters, JCIS Open 9 (2023) 100075, https://doi.org/10.1016/j.jciso.2023.100075.

[16] J. Li, Z. Wang, H. Zhang, J. Gao, A. Zheng, Progress in the development of stabilization strategies for nanocrystal preparations, Drug Deliv. 28 (1) (2021) 19–36, https://doi.org/10.1080/10717544.2020.1856224.

[17] M.B. McGuckin, J. Wang, R. Ghanma, N. Qin, S.D. Palma, R.F. Donnelly, A. J. Paredes, Nanocrystals as a master key to deliver hydrophobic drugs via multiple administration routes, J. Control. Release 345 (2022) 334–353, https://doi.org/10.1016/j.jconrel.2022.03.012.

[18] M. Singhal, A. Baumgartner, E. Turunen, B. van Veen, J. Hirvonen, L. Peltonen, Nanosuspensions of a poorly soluble investigational molecule ODM-106: impact of milling bead diameter and stabilizer concentration, Int. J. Pharm. 587 (2020) 119636, https://doi.org/10.1016/j.ijpharm.2020.119636.

[19] M. Li, N. Yaragudi, A. Afolabi, R. Dave, E. Bilgili, Sub-100nm drug particle suspensions prepared via wet milling with low bead contamination through novel process intensification, Chem. Eng. Sci. 130 (2015) 207–220, https://doi.org/10.1016/j.ces.2015.03.020.

[20] A.H. Abdelhameed, W.A. Abdelhafez, K.I. Saleh, A.A. Hamad, M.S. Mohamed, Formulation and optimization of oral fast dissolving films loaded with nanosuspension to enhance the oral bioavailability of Fexofenadine HCL, J. Drug Deliv. Sci. Technol. 85 (2023) 104578, https://doi.org/10.1016/j.jddst.2023.104578.

[21] P. Suriyaamporn, C. Pornpitchanarong, B. Pamornpathomkul, P. Patrojanasophon, T. Rojanarata, P. Opanasopit, T. Ngawhirunpat, Ganciclovir nanosuspension-loaded detachable microneedles patch for enhanced drug delivery to posterior eye segment, J. Drug Deliv. Sci. Technol. 88 (2023) 104975, https://doi.org/10.1016/j.jddst.2023.104975.

[22] Y. Liu, Z. Zhang, C. Wang, X. Xie, Y. Ma, Y. Wang, Biodegradable and dissolvable resveratrol nanocrystals non-silicon microneedles for transdermal drug delivery, J. Drug Deliv. Sci. Technol. 86 (2023) 104653, https://doi.org/10.1016/j.jddst.2023.104653.

[23] Q. Ran, M. Wang, W. Kuang, J. Ouyang, D. Han, Z. Gao, J. Gong, Advances of combinative nanocrystal preparation technology for improving the insoluble drug solubility and bioavailability, Crystals 12 (2022) 1200, https://doi.org/10.3390/cryst12091200.

[24] A. Homayouni, F. Sadeghi, J. Varshosaz, H.A. Garekani, A. Nokhodchi, Promising dissolution enhancement effect of soluplus on crystallized celecoxib obtained through antisolvent precipitation and high pressure homogenization techniques, Colloids Surf. B Biointerfaces 122 (2014) 591–600, https://doi.org/10.1016/j.colsurfb.2014.07.037.

[25] B. Sinha, R.H. Müller, J.P. Möschwitzer, Bottom-up approaches for preparing drug nanocrystals: formulations and factors affecting particle size, Int. J. Pharm. 453 (2013) 126–141, https://doi.org/10.1016/j.ijpharm.2013.01.019.

[26] Y. Dong, W.K. Ng, J. Hu, S. Shen, R.B. Tan, A continuous and highly effective static mixing process for antisolvent precipitation of nanoparticles of poorly water-soluble drugs, Int. J. Pharm. 386 (1-2) (2010) 256–261, https://doi.org/10.1016/j.ijpharm.2009.11.007.

[27] J.P. Martins, G. Torrieri, H.A. Santos, The importance of microfluidics for the preparation of nanoparticles as advanced drug delivery systems, Expert Opin. Drug Deliv. 15 (5) (2018) 469–479, https://doi.org/10.1080/17425247.2018.1446936.

[28] Z. Whiteley, H.M.K. Ho, Y.X. Gan, L. Panariello, G. Gkogkos, A. Gavriilidis, D.Q. M. Craig, Microfluidic synthesis of protein-loaded nanogels in a coaxial flow reactor using a design of experiments approach, Nanoscale Adv. 3 (2021) 2039–2055, https://doi.org/10.1039/D0NA01051K.

[29] G. Whitesides, The origins and the future of microfluidics, Nature 442 (2006) 368–373, https://doi.org/10.1038/nature05058.

[30] J. Lu, J. Yan, Y. Guo, J. Qiu, S. Zhao, B. Bao, Controlling solid form and crystal habit of triphenylmethanol by antisolvent crystallization in a microfluidic device, Chin. Chem. Lett. 35 (4) (2024) 108876, https://doi.org/10.1016/j.cclet.2023.108876.

[31] D. Liu, H. Zhang, F. Fontana, J.T. Hirvonen, H.A. Santos, Current developments and applications of microfluidic technology toward clinical translation of nanomedicines, Adv. Drug Deliv. Rev. 128 (2018) 54–83, https://doi.org/10.1016/j.addr.2017.08.003.

[32] A. Saikia, R. Newar, S. Das, A. Singh, D.J. Deuri, A. Baruah, Scopes and challenges of microfluidic technology for nanoparticle synthesis, photocatalysis and sensor applications: a comprehensive review, Chem. Eng. Res. Des. 193 (2023) 516–539, https://doi.org/10.1016/j.cherd.2023.03.049.

[33] L. Zhang, S. Mao, Application of quality by design in the current drug development, Asian J. Pharm. Sci. 12 (2017) 1–8, https://doi.org/10.1016/j.ajps.2016.07.006.

[34] E. Pallagi, R. Ismail, T.L. Paál, I. Csóka, Initial risk assessment as part of the quality by design in peptide drug containing formulation development, Eur. J. Pharm. Sci. 122 (2018) 160–169, https://doi.org/10.1016/j.ejps.2018.07.003.

[35] P. Lhaglham, L. Jiramonai, Y. Jia, B. Huang, Y. Huang, X. Gao, J. Zhang, X.J. Liang, M. Zhu, Drug nanocrystals: surface engineering and its applications in targeted delivery, iSci 27 (11) (2024) 111185, https://doi.org/10.1016/j.isci.2024.111185.

[36] N. Anup, S. Thakkar, M. Misra, Formulation of olanzapine nanosuspension based orally disintegrating tablets (ODT); comparative evaluation of lyophilization and electrospraying process as solidification techniques, Adv. Powder Technol. 29 (8) (2018) 1913–1924, https://doi.org/10.1016/j.apt.2018.05.003.

[37] E. Jakubowska, M. Bielejewski, B. Milanowski, J. Lulek, Freeze-drying of drug nanosuspension– study of formulation and processing factors for the optimization and characterization of redispersible cilostazol nanocrystals, J. Drug Deliv. Sci. Technol. 74 (2022) 103528, https://doi.org/10.1016/j.jddst.2022.103528.

[38] S. Thakkar, M. Misra, Electrospray drying of docetaxel nanosuspension: a study on particle formation and evaluation of nanocrystals thereof, J. Drug Deliv. Sci. Technol. 60 (2020) 102009, https://doi.org/10.1016/j.jddst.2020.102009.

[39] Y. Ding, T. Zhao, J. Fang, J. Song, H. Dong, J. Liu, S. Li, M. Zhao, Recent developments in the use of nanocrystals to improve bioavailability of, APIs WIREs Nanomed. Nanobiotechnol. 16 (2) (2024) e1958, https://doi.org/10.1002/wnan.1958.

[40] J.A. Davidson, L. Sloan, Fixed-dose combination of Canagliflozin and Metformin for the treatment of Type 2 Diabetes: an overview, Adv. Ther. 34 (1) (2017) 41–59, https://doi.org/10.1007/s12325-016-0434-2.

[41] B.L. Neuen, T. Young, H.J.L. Heerspink, B. Neal, V. Perkovic, L. Billot, K. W. Mahaffey, D.M. Charytan, D.C. Wheeler, C. Arnott, S. Bompoint, A. Levin, M. J. Jardine, SGLT2 inhibitors for the prevention of kidney failure in patients with type 2 diabetes: a systematic review and meta-analysis, Lancet Diabetes Endocrinol. 7 (2019) 845–854, https://doi.org/10.1016/S2213-8587(19)30256-6.

[42] G.D. Lopaschuk, S. Verma, Mechanisms of cardiovascular benefits of sodium glucose Co-Transporter 2 (SGLT2) inhibitors, A StateArt. Rev. JACC Basic Transl. Sci. 5 (6) (2020) 632–644, https://doi.org/10.1016/j.jacbts.2020.02.004.

[43] A.S. Alshnbari, S.A. Millar, S.E. O'Sullivan, I. Idris, Effect of Sodium-glucose cotransporter-2 inhibitors on endothelial function: a systematic review of preclinical studies, Diabetes Ther. 11 (9) (2020) 1947–1963, https://doi.org/10.1007/s13300-020-00885-z.

[44] Food and Drug Administration, Center For Drug Evaluation And Research. Application Number: 205879Orig1s000. Canagliflozin Chemistry Review(s). 2016, 1-33. Available fromhttps://www.accessdata.fda.gov/drugsatfda_docs/nda/2016/205879Orig1s000ChemR.pdf.

[45] K. Shoda, S. Tsuji, S. Nakamura, Y. Egashira, Y. Enomoto, N. Nakayama, M. Shimazawa, T. Iwama, H. Hara, Canagliflozin inhibits glioblastoma growth and proliferation by activating AMPK, Cell Mol. Neurobiol. 43 (2023) 879–892, https://doi.org/10.1007/s10571-022-01221-8.

[46] D. Xu, Y. Zhou, X. Xie, L. He, J. Ding, S. Pang, B. Shen, C. Zhou, Inhibitory effects of canagliflozin on pancreatic cancer are mediated via the downregulation of glucose transporter-1 and lactate dehydrogenase A, Int. J. Oncol. (2020) 1223–1233, https://doi.org/10.3892/ijo.2020.5120, 57(5.
[47] O.D. Biziotis, E.E. Tsakiridis, A. Ali, E. Ahmadi, J. Wu, S. Wang, B. Mekhaeil, K. Singh, G. Menjolian, T. Farrell, B. Abdulkarim, R.K. Sur, A. Mesci, P. Ellis, T. Berg, J.L. Bramson, P. Muti, G.R. Steinberg, T. Tsakiridis, Canagliflozin mediates tumor suppression alone and in combination with radiotherapy in non-small cell lung cancer (NSCLC) through inhibition of HIF-1α, Mol. Oncol. 17 (2023) 2235–2256, https://doi.org/10.1002/1878-0261.13508.
[48] Y. Wang, L. Yang, L. Mao, L. Zhang, Y. Zhu, Y. Xu, Y. Cheng, R. Sun, Y. Zhang, J. Ke, D. Zhao, SGLT2 inhibition restrains thyroid cancer growth via G1/S phase transition arrest and apoptosis mediated by DNA damage response signaling pathways, Cancer Cell. Int. 22 (2022) 74, https://doi.org/10.1186/s12935-022-02496-z.
[49] European Medicines Agency, Committee for Medicinal Products for Human Use (CHMP), Assesment report Canagliflozin. Available fromhttps://www.ema.europa.eu/en/documents/assessment-report/invokana-epar-public-assessment-report_en.pdf.
[50] Y. Pirincci-Tok, B. Mesut, S. Güngör, A.O. Sarıkaya, E.E. Aldeniz, U. Dude, Y. Özsoy, Systematic screening study for the selection of proper stabilizers to produce physically stable Canagliflozin nanosuspension by wet milling method, Bioeng 10 (2023) 927, https://doi.org/10.3390/bioengineering10080927.
[51] J. Pielenhofer, S.L. Meiser, K. Gogoll, A.M. Ciciliani, M. Denny, M. Klak, B.M. Lang, P. Staubach, S. Grabbe, H. Schild, M.P. Radsak, H. Spahn-Langguth, P. Langguth, Quality by design (QbD) approach for a nanoparticulate imiquimod formulation as an investigational medicinal product, Pharmaceutics 15 (2023) 514, https://doi.org/10.3390/pharmaceutics15020514.
[52] H. Kathpalia, S. Juvekar, K. Mohanraj, M. Apsingekar, S. Shidhaye, Investigation of pre-clinical pharmacokinetic parameters of atovaquone nanosuspension prepared using a pH-based precipitation method and its pharmacodynamic properties in a novel artemisinin combination, J. Glob. Antimicrob. Resist. 22 (2020) 248–256, https://doi.org/10.1016/j.jgar.2020.02.018.
[53] I. Aghrbi, V. Fülöp, G. Jakab, N. Kállai-Szabó, E. Balogh, I. Antal, Nanosuspension with improved saturated solubility and dissolution rate of cilostazol and effect of solidification on stability, J. Drug Deliv. Sci. Technol. 61 (2021) 102165, https://doi.org/10.1016/j.jddst.2020.102165.
[54] M. Wewers, S. Czyz, J.H. Finke, E. John, B. Van Eerdenbrugh, M. Juhnke, H. Bunjes, A. Kwade, Influence of formulation parameters on redispersibility of naproxen nanoparticles from granules produced in a fluidized bed process, Pharmaceutics 12 (2020) 363, https://doi.org/10.3390/pharmaceutics12040363.
[55] S. Jain, V.A. Reddy, S. Arora, K. Patel, Development of surface stabilized candesartan cilexetil nanocrystals with enhanced dissolution rate, permeation rate across Caco-2, and oral bioavailability, Drug Deliv. Transl. Res. 6 (5) (2016) 498–510, https://doi.org/10.1007/s13346-016-0297-8.
[56] R.H. Müller, C.M. Keck, Twenty years of drug nanocrystals: where are we, and where do we go? Eur. J. Pharm. Biopharm.. 80 (1) (2012) 1–3, https://doi.org/10.1016/j.ejpb.2011.09.012.
[57] U.S. Food and Drug Administration, Approval Package for NDA 204042/S-026: Invokana (canagliflozin) tablets (Supplement Approval), Silver Spring, MD, 25 Jul 2017. Available from:https://www.accessdata.fda.gov/drugsatfda_docs/nda/2017/204042Orig1s026.pdf.
[58] M. Azad, J. Moreno, E. Bilgili, R. Davé, Fast dissolution of poorly water soluble drugs from fluidized bed coated nanocomposites: impact of carrier size, Int. J. Pharm. 513 (1–2) (2016) 319–331, https://doi.org/10.1016/j.ijpharm.2016.09.046.
[59] M.F. Simões, G. Silva, A.C. Pinto, M. Fonseca, N.E. Silva, R.M.A. Pinto, S. Simões, Artificial neural networks applied to quality-by-design: from formulation development to clinical outcome, Eur. J. Pharm. Biopharm. 152 (2020) 282–295, https://doi.org/10.1016/j.ejpb.2020.05.012.
[60] H. Rachmawati, A. Rahma, L. Al Shaal, R.H. Müller, C.M. Keck, Destabilization mechanism of ionic surfactant on curcumin nanocrystal against electrolytes, Sci. Pharm. 84 (4) (2016) 685–693, https://doi.org/10.3390/scipharm84040685.
[61] United States Pharmacopeial Convention, United States Pharmacopeia–National Formulary (USP–NF), Online Edition, Rockville, MD, USA. Available from: https://online.uspnf.com/uspnf/document/1_GUID-DA161518-EC27-4647-AACD-29D28F2A4E92_7_en-US(accessed [12.12.2025]).
[62] International Conference on Harmonisation of Technical Requirements for Registration of Pharmaceuticals for Human Use (ICH). (2009). ICH Harmonised Tripartite Guideline: Quality Risk Management Q9(R1). Available fromhttps://database.ich.org/sites/default/files/ICH_Q9%28R1%29_Guideline_Step4_2025_0115.pdf.
[63] International Conference on Harmonisation of Technical Requirements for Registration of Pharmaceuticals for Human Use (ICH). (2009). ICH Harmonised Tripartite Guideline: Quality Risk Management Q9(R1). Available fromhttps://database.ich.org/sites/default/files/ICH_Q9%28R1%29_Guideline_Step4_2025_0115.pdf.
[64] M.S. Khan, P.R. Ravi, D.S. Dhavan, Design, optimization, in vitro and in vivo evaluation of triamcinolone acetonide nanocrystals loaded in situ gel for topical ocular delivery, Colloids Surf. B Biointerfaces 231 (2023) 113539, https://doi.org/10.1016/j.colsurfb.2023.113539.
[65] F. Shaikh, M. Patel, V. Patel, A. Patel, G. Shinde, S. Shelke, I. Pathan, Formulation and optimization of cilnidipine loaded nanosuspension for the enhancement of solubility, dissolution and bioavailability, J. Drug Deliv. Sci. Technol. 69 (2022) 103066, https://doi.org/10.1016/j.jddst.2021.103066.
[66] D.H. Kuk, E.S. Ha, D.H. Ha, W.Y. Sim, S.K. Lee, J.S. Jeong, J.S. Kim, I.H. Baek, H. Park, D.H. Choi, J.W. Yoo, S.H. Jeong, S.J. Hwang, M.S. Kim, Development of a Resveratrol nanosuspension using the antisolvent precipitation method without solvent removal, based on a quality by design (QbD) Approach, Pharmaceutics 11 (2019) 688, https://doi.org/10.3390/pharmaceutics11120688.
[67] K. Kadota, S. Nogami, H. Uchiyama, Y. Tozuka, Controlled release behavior of curcumin from kappa-carrageenan gels with flexible texture by the addition of metal chlorides, Food Hydrocoll. 101 (2020) 105564, https://doi.org/10.1016/j.foodhyd.2019.105564.
[68] M. Malamatari, S. Somavarapu, K. Kachrimanis, G. Buckton, K.M.G. Taylor, Preparation of respirable nanoparticle agglomerates of the low melting and ductile drug ibuprofen: impact of formulation parameters, Powder Technol. 308 (2017) 123–134, https://doi.org/10.1016/j.powtec.2016.12.007.
[69] P. Vass, B. Démuth, A. Farkas, E. Hirsch, E. Szabó, B. Nagy, S.K. Andersen, T. Vigh, G. Verreck, I. Csontos, G. Marosi, Z.K. Nagy, Continuous alternative to freeze drying: manufacturing of cyclodextrin-based reconstitution powder from aqueous solution using scaled-up electrospinning, J. Control. Release 298 (2019) 120–127, https://doi.org/10.1016/j.jconrel.2019.02.019.
[70] S. Zhao, C. Huang, X. Yue, X. Li, P. Zhou, A. Wu, C. Chen, Y. Qu, C. Zhang, Application advance of electrosprayed micro/nanoparticles based on natural or synthetic polymers for drug delivery system, Mater. Des. 220 (2022) 110850, https://doi.org/10.1016/j.matdes.2022.110850.
[71] B.S. Zorec, Š. Zupančič, Z. Lavrič, R. Dreu, Particle properties and drug metastable solubility of simvastatin containing PVP matrix particles prepared by electrospraying technique, Eur. J. Pharm. Sci. 158 (2021) 105649, https://doi.org/10.1016/j.ejps.2020.105649.
[72] A.M. Vorobei, M.O. Kostenko, O.O. Parenago, Viscosity measurement of CO2–solvent mixtures for the study of the morphology and size of crystalline particles obtained using supercritical antisolvent precipitation, Materials 16 (2023) 6151, https://doi.org/10.3390/ma16186151.
[73] A.M.dos Santos, A.B. Meneguin, B. Fonseca-Santos, M.P.C. de Souza, L.M. B. Ferreira, R.M. Sábio, M. Chorilli, M.P.D. Gremião, The role of stabilizers and mechanical processes on physico-chemical and anti-inflammatory properties of methotrexate nanosuspensions, J. Drug Deliv. Sci. Technol. 57 (2020) 101638, https://doi.org/10.1016/j.jddst.2020.101638.
[74] M.A. Khan, M.M. Ansari, S.T. Arif, A. Raza, H.I. Choi, C.W. Lim, H.Y. Noh, J.S. Noh, S. Akram, H.A. Nawaz, M. Ammad, A.A. Alamro, A.A. Alghamdi, J.K. Kim, A. Zeb, Eplerenone nanocrystals engineered by controlled crystallization for enhanced oral bioavailability, Drug Deliv. 28 (2021) 2510–2524, https://doi.org/10.1080/10717544.2021.2008051.
[75] H.S.M. Ali, P. York, N. Blagden, N, Preparation of hydrocortisone nanosuspension through a bottom-up nanoprecipitation technique using microfluidic reactors, Int. J. Pharm. 375 (1-2) (2009) 107–113, https://doi.org/10.1016/j.ijpharm.2009.03.029.
[76] S. Zhao, Y. Wei, P. Yu, F. Yuan, C. Li, Q. Gao, L. Sheng, Y. Feng, J. Yang, W. He, N. Zhu, Y. Li, D. Ji, K. Guo, High throughput preparation and particle size control strategy of nano apigenin by a scale-up microreactor, J. Ind. Eng. Chem. 133 (2024) 207–218, https://doi.org/10.1016/j.jiec.2023.11.059.
[77] B.Y. Gajera, D.A. Shah, R.H. Dave, Development of an amorphous nanosuspension by sonoprecipitation-formulation and process optimization using design of experiment methodology, Int. J. Pharm. 559 (2019) 348–359, https://doi.org/10.1016/j.ijpharm.2019.01.054.
[78] J. Kim, D.G. Kim, K.H. Ryu, Enhancing response surface methodology through coefficient clipping based on prior knowledge, Processes 11 (2023) 3392, https://doi.org/10.3390/pr11123392.
[79] V.C. Gurumukhi, V.P. Sonawane, G.G. Tapadiya, S.B. Bari, S.J. Surana, S. S. Chalikwar, Quality-by-design based fabrication of febuxostat-loaded nanoemulsion: statistical optimization, characterizations, permeability, and bioavailability studies, Heliyon 9 (4) (2023) e15404, https://doi.org/10.1016/j.heliyon.2023.e15404.
[80] L.C. Henríquez, B. Bahloul, K. Alhareth, F. Oyoun, M. Frejková, L. Kostka, T. Etrych, L. Kalshoven, A. Guillaume, N. Mignet, Y. Corvis, Step-by-step standardization of the bottom-up semi-automated nanocrystallization of pharmaceuticals: a quality by design and design of experiments joint approach, Small 20 (2024) 2306054, https://doi.org/10.1002/smll.202306054.
[81] E. Jakubowska, B. Milanowski, J. Lulek, Systematic approach to the development of cilostazol nanosuspension by liquid antisolvent precipitation (LASP) and its combination with ultrasound, Int. J. Mol. Sci. 22 (2021) 12406, https://doi.org/10.3390/ijms222212406.
[82] C. Morikawa, K. Ueda, M. Omori, K. Higashi, K. Moribe, Formation mechanism of amorphous drug nanoparticles using the antisolvent precipitation method elucidated by varying the preparation temperature, Int. J. Pharm. 610 (2021) 121210, https://doi.org/10.1016/j.ijpharm.2021.121210.
[83] E. Pardhi, Y. Bhor, P.K. Singh, N.K. Mehra, An apprise on novel drug delivery systems for management of diabetes mellitus, J. Drug Deliv. Sci. Technol. 94 (2024) 105473, https://doi.org/10.1016/j.jddst.2024.105473.
[84] E. Browne, R. Charifou, Z.A. Worku, R.P. Babu, A.M. Healy, Amorphous solid dispersions of ketoprofen and poly-vinyl polymers prepared via electrospraying and spray drying: a comparison of particle characteristics and performance, Int. J. Pharm. 566 (2019) 173–184, https://doi.org/10.1016/j.ijpharm.2019.05.062.
[85] X. Zhang, J. Guan, R. Ni, L.C. Li, S. Mao, Preparation and solidification of redispersible nanosuspensions, J. Pharm. Sci. 103 (7) (2014) 2166–2176, https://doi.org/10.1002/jps.24015.
[86] W. Abdelwahed, G. Degobert, S. Stainmesse, H. Fessi, Freeze-drying of nanoparticles: formulation, process and storage considerations, Adv. Drug Deliv. Rev. 58 (15) (2006) 1688–1713, https://doi.org/10.1016/j.addr.2006.09.017.

[87] H.P. Diogo, J.J.M. Ramos, Molecular mobility in Soluplus, a polymer with extremely low dynamic fragility; a study by thermally stimulated depolarization currents, J. Non-Cryst. Solids 591 (2022) 121738, https://doi.org/10.1016/j.jnoncrysol.2022.121738.
[88] H. Chen, M. Deng, L. Xie, K. Liu, X. Zhang, X. Li, Preparation and characterization of quercetin nanosuspensions using gypenosides as novel stabilizers, J. Drug Deliv. Sci. Technol. 67 (2022) 102962, https://doi.org/10.1016/j.jddst.2021.102962.
[89] M. Elmowafy, K. Shalaby, M.M. Al-Sanea, O.M. Hendawy, A. Salama, M.F. Ibrahim, M.M. Ghoneim, Influence of stabilizer on the development of luteolin nanosuspension for cutaneous delivery: an in vitro and in vivo evaluation, Pharmaceutics 13 (2021) 1812, https://doi.org/10.3390/pharmaceutics13111812.
[90] A.H. Ibrahim, E. Rosqvist, J.H. Smått, H.M. Ibrahim, H.R. Ismael, M.I. Afouna, A. M. Samy, J.M. Rosenholm, Formulation and optimization of lyophilized nanosuspension tablets to improve the physicochemical properties and provide immediate release of silymarin, Int. J. Pharm. 563 (2019) 217–227, https://doi.org/10.1016/j.ijpharm.2019.03.064.
[91] N. C. Patel and H. A. Patel, A Recent Solidification Approach for Nanosuspension: Formulation, Optimisation and Evaluation of Canagliflozin Immediate Release Pellets, Folia Med. 64(3):488-500. https://doi.org/10.3897/folmed.64.e68866.
[92] E. Gomaa, M.S. Attia, F.E.S. Ghazy, A.E.A. Hassan, A.A. Hasan, Pump-free electrospraying: a novel approach for fabricating Soluplus®-based solid dispersion nanoparticles, J. Drug Deliv. Sci. Technol. 67 (2022) 103027, https://doi.org/10.1016/j.jddst.2021.103027.